Università degli Studi di Cagliari
Dipartimento di Ingegneria Meccanica
Dottorato di Ricerca in Progettazione Meccanica
XX Ciclo – Ing–Ind/11

Experimental and Numerical Analysis of Heat Transfer and Airflow on an Interactive Building Facade

Roberto Fuliotto

Supervisor:
Prof. Natalino Mandas

Co–supervisor:
Prof. Qingyan Chen
Dr. Francesco Cambuli

January 2008
Thesis for the Degree of Doctor of Philosophy

Dipartimento di Ingegneria Meccanica, DIMeCa
Università degli Studi di Cagliari
Piazza d'Armi, 1
09123 Cagliari, Italy

Roberto Fuliotto
Printed in Italy
DIMeCa-PhD 2004-2007 – XX Ciclo

`fuliotto@dimeca.unica.it`

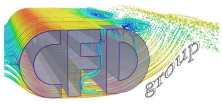

A thesis submitted in partial fulfillment of the requirements of the degree of Doctor of Philosophy at the University of Cagliari

This research project has been funded by a grant
from the "*Banco di Sardegna Foundation*"

This thesis has been written in American English and typeset using LaTeX 2_ε. Illustrations have been drawn with MS Office, graphs and plots have been created with Matlab, Gnuplot, MS Excel and TecPlot

The front cover picture shows a view of Chicago, IL,
from the bridge on the Michigan Avenue

Acknowledgment

First, I would like to thank Prof. Natalino Mandas, my mentor during these years, who gave me the opportunity to challenge myself through a Ph.D. I would also like to recognize Dr. Francesco Cambuli for his enormous help and close friendship during the difficult moments that CFD generated.

I am extremely indebted to Prof. Qingyan Chen at Purdue University for sharing with me his expertise in this technical field, as well as his hospitality in hosting me as a visiting scholar over two periods at Purdue University. I would also like to thank his wife and him for their great sense of hospitality and friendship.

I would like to extend my thanks to Giampiero Manara, head of the Permasteelisa R&D Department, for making available his company's information about the experimental campaign, and to Nicoletta Bacchin for her contribution on the experimental data interpretation.

I must also not forget my friends and colleagues of the D.I.Me.Ca.–CFD group: Giorgio Crasto, Giorgio Melis and Marco Pau. A special mention has to be provided for Carlo Enrico Carcangiu, I could have wished for no better friend during these "basement-years" work. It was a great working group and it has been an honor to be a friend and to work with each of these guys.

Speaking of colleagues/friends, I have to say thank you to all the fellows that I met at the Herrick's Lab and especially Sagnik Mazumdar, Zhao Zhang and Ling Feng Ma. I am also grateful to all the other friends that I have met in the U.S. Living abroad was sometime difficult, but with them everything was easier!

I would also like to salut colleagues and friends of the other D.I.Me.Ca. research groups for their always ready help whenever I needed advice out of my research field and for the great breakfasts we used to have.

Finally I have to virtually hug Valeria, my parents and my brother Marco for the unfailing support they gave me during these years.

Many thanks to everyone!

Cagliari, January 23^{rd}*, 2008*

Roberto

To Valeria

"When I meet God, I am going to ask him two questions: Why relativity? And why turbulence? I really believe he will have an answer for the first"
Werner Karl Heisenberg (1901 – 1976)

Abstract

Architectural trend during last decade leads toward new concepts of building practice. Even more designers embeds the use of high technology features in their projects for both aesthetic and technical aims. The actual international concern about energy and environment problems is a major motivating force to include in modern design a deep analysis of the energetic behavior of the building.

The designer desire to improve the transparency of the facade as aesthetic feature and the technical need to improve indoor environment, acoustic and energy reduction drive toward the concept of *Double Skin Facade* (DSF). DSF have, in this sense, an ever greater importance because of their common presence in architectural competition all over the world. Unfortunately there are still relatively few buildings in which they have actually realized and it would be important to understand the real operating behavior in order to be able to choose the best typology in function of the specific location and environmental conditions.

Also the growing interest toward the concept of energy saving building it is moving the interest of worldwide researchers to improve the quality of the analysis in terms both of results and operative time. Define a mathematical model to simplify the real model seem to be the most reliable and economic approach.

The use of heat transfer methods, strictly linked to fluid dynamics equations, could be a comprehensive suitable method to understand the functionality of the double facades. At the moment only few analytical models based on empirical calculations could help both the designer and the constructor in the building process.

The use of the *Computational Fluid Dynamic* (CFD) can be the tool for a more inclusive approach that could lead to the definition of any empirical formulation that could define, with an acceptable, known error, the behavior of the double facade in its operation environment. The CFD process can not be accurately performed without steady basis firstly funded over a validation process and then over an optimization of the double-skin facades typologies.

The purpose of this work is to produce a comprehensive CFD analysis to understand double-skin facades behavior in the different environmental conditions that could be a background for the development of an easy-to-use tool

for designers that are approaching to the problem without specific thermo fluid dynamics knowledge.

The DSF has very complex thermo-fluid phenomena under the outdoor environmental conditions, which involve conductive, convective, and radiative heat transfer with laminar, transient, and turbulent flow regimes. In order to develop a suitable computer procedure that is capable to accurately calculate the phenomena, a full scale test room has been constructed to collect data for validating the procedure.

The test room envelope is an instrumented and monitored DSF with integrated Venetian blinds in the ventilated cavity. For different layers of the facade the following parameters have been stored: facade temperatures, transmitted solar radiation through facade, airflow rate and temperature. Moreover, a meteorological station has recorded outdoor climatic data.

The experimental data has been used to validate a CFD simulation solving the governing equations for a fluid following the density Boussinesq model, with the two–equations, eddy–viscosity RNG k–ϵ turbulence model.

A decoupled method for the radiative heat transfer has been implemented. Firstly, the global net energy balance and the optical properties of the DSF were evaluated from the measured data. Then a CFD software has been used to calculate temperature and flow distributions in the DSF, based on the source terms previously evaluated under different scenarios with varying weather conditions and solar radiation.

The results show that the thermo–fluid phenomena can be approximated to be two dimensional. The CFD can calculate the temperature distribution in the DSF with reasonably good accuracy. The results also show that the decoupled method for radiative heat transfer is reasonable acceptable for such an advanced DSF.

Sommario

Lo scopo fondamentale del progetto è quello di simulare mediante la CFD (*Computational Fluid Dynamics*) il fenomeno fisico che caratterizza gli scambi termici globali di una facciata interattiva in doppia pelle di vetro (*Double Skin Facade*, DSF) per individuare i parametri necessari per una corretta modellazione di questi sistemi.

Gli standard architettonici attuali hanno guidato gli architetti verso nuovi concetti di pratica edilizia utilizzando gli ultimi ritrovati tecnici per scopi sia estetici che prettamente tecnici. Il desiderio del progettista di unire l'esigenza estetica di estremizzare la trasparenza e la richiesta tecnica di ottimizzazione dell'ambiente interno in termini energetici e acustici porta verso il concetto di DSF. Con la ratifica del Protocollo di Kyoto per la riduzione delle emissioni dei gas che favoriscono l'effetto serra le diverse entità governative hanno istituito commissioni e promosso progetti di ricerca per cercare di migliorare uno dei punti chiave, ossia la diminuzione del consumo energetico. A tal fine l'involucro edilizio degli edifici svolge un compito fondamentale in quanto interfaccia naturale tra l'ambiente interno e l'ambiente esterno. Così a partire dall'Agenzia Internazionale per l'Energia (IEA) fino ad arrivare all'Ente per le Nuove tecnologie, l'Energia e l'Ambiente (ENEA), si sono visti prolificare i progetti di ricerca per l'ottimizzazione delle tecniche di risparmio energetico negli edifici. In questo contesto di interesse internazionale si inserisce l'analisi di nuove tecniche e tecnologie intelligenti applicate all'involucro edilizio, capaci di adattarsi in maniera automatica o semi-automatica alle variazioni dell'ambiente esterno esattamente come le DSF.

In generale, una DSF è composta essenzialmente da due vetri paralleli separati da una cavità, l'insieme costituisce una chiusura verticale di un edificio. Ognuna di queste vetrate è comunemente chiamata *pelle* (skin) o *strato* (layer). La cavità racchiusa dalle due pelli può essere ventilata o meno e può avere differenti ampiezze a partire da pochi centimetri fino a qualche metro, in funzione dell'utilizzo e della tipologia della facciata stessa, nonché del tipo di ventilazione adottata. Alla DFS può essere associato un meccanismo oscurante (blinder) che garantisce una barriera all'irraggiamento solare. Il progetto di ricerca si prefigge lo scopo di valutare mediante un codice fluidodinamico le caratteristiche termo–fluidodinamiche della DSF. La difficoltà intrinseca del problema riguarda la complessità del fenomeno fisico che determina il funzionamento

della facciata stessa. Oltre alla trasmissione del calore per conduzione si innescano fenomeni di trasmissione per convezione mista e di irraggiamento che complicano il modello matematico e la sua modellazione numerica.

L'analisi CFD non può essere affrontata prima di aver effettuato un processo di validazione che ne verifichi l'efficacia. La validazione è stata effettuata seguendo una procedura step–by–step a partire da dati sperimentali e numerici di casi che rapresentassero singolarmente i fenomeni presenti nella DSF.

A seguire sono stati analizzati i dati sperimentali forniti dal Research & Development Department della Permasteelisa S.p.A multinazionale leader nel settore della produzione di involucri vetrati per edifici, su un particolare tipo di DSF la Facciata Interattiva (Interactive Facade) strumentata e testata a San Vendemiano (VI) nel campus della società. La DSF era costituita da un vetro di protezione esterno e un doppio vetro sul lato interno. La cavità, ventilata meccanicamente mediante piccoli ventilatori centrifughi, era dotata di una veneziana per l'oscuramento ad azionamento automatico o manuale.

Lo scambio termico della DSF è caratterizzato e influenzato nella maggior parte dall'irraggiamento solare. Lo scambio termico radiativo è stato *disaccoppiato* calcolando separatamente l'apporto energetico dovuto alla radiazione solare in ogni singolo strato e successivamente introdotto nella simulazione CFD. Il metodo di disaccoppiamento prevede due fasi distinte. Nella prima fase vengono calcolate le proprietà ottiche della DSF mediante il software WIS sviluppato attraverso il progetto *Advanced Windows Information System* (WIS). Nella seconda fase, mediante i dati ottenuti dal WIS, è stato possibile ricostruire il bilancio energetico della facciata ed è stata determinata la quantità di energia assorbita da ogni strato della DSF. Questi valori opportunamente elaborati sono stati utilizzati nel codice CFD per poter effettuare le simulazioni.

Il confronto con i dati sperimentali ha permesso di trovare un compromesso tra l'accuratezza dei risultati numerici e i tempi di calcolo. E' stato possibile appurare che si può ridurre il modello tridimensionale a bidimensionale, anche se il primo permette una migliore descrizione dei fenomeni che si verificano nella DSF.

La ricerca del compromesso tra accuratezza e tempi di calcolo è stato cercato per creare una solida base per lo sviluppo futuro di ulteriori analisi per la definizione di un database costituito dai risultati di una parametrizzazione delle DSF nelle diverse configurazioni geometriche, climatiche ed energetiche. L'obbiettivo sarà quello di fornire uno strumento per il progettista e il costruttore che permetta di effettuare le scelte progettuali con procedure semplificate mediante una parametrizzazione delle caratteristiche geometriche, climatiche e energetiche.

Contents

CONTENTS

Nomenclature

Acronyms

CFD	Computational Fluid Dynamics
DSF	Double Skin Facade
RANS	Reynolds Averaged Navier Stokes
RNG	Re–Normalized Group
SHGC	Solar Heat Gain Coefficient
VT	Visible Transmittance

Latin letters

A	Area	$[m^2]$
A_{pf}	Projected area of fenestration	$[m^2]$
C_p	Specific heat at constant pressure	$[Jkg^{-1}K^{-1}]$
E_b	Emissive power of blackbody	$[Wm^{-2}]$
$\mathscr{F}$	Geometric shape factor for radiation	
g	Acceleration due to the gravity	$[mm^{-2}]$
H	Height	$[m]$
h_c	Convective heat transfer coefficient	$[Wm^{-1}K^{-2}]$
h_r	Radiative heat transfer coefficient	$[Wm^{-1}K^{-2}]$
I	Irradiation incident on unit surface on unit of time	$[Wm^{-2}]$
I_b	Direct Beam irradiation	$[Wm^{-2}]$
I_s	Sky or diffuse irradiation	$[Wm^{-2}]$
I_g	Ground reflected irradiation	$[Wm^{-2}]$
k	Thermal conductivity	$[Wm^{-1}K^{-1}]$
L	Characteristic length	$[m]$
q	Heat flux	$[Wm^{-2}]$

q_c	Rate of heat flow by convection	$[W]$
q_k	Rate of heat flow by conduction	$[W]$
q_r	Rate of heat flow by radiation	$[W]$
T	Temperature	$[^oC, K]$
T_g	Glass temperature	$[^oC, K]$
T_o	Inlet temperature	$[^oC, K]$
T_s	Surface temperature	$[^oC, K]$
$T_V B$	Venetian blinder slat temperature	$[^oC, K]$
T_∞	Free stream temperature	$[^oC, K]$
U	Overall coefficient of heat transfer	$\left[Wm^{-1}K^{-2}\right]$
V	Velocity	$\left[ms^{-1}\right]$
x	Coordinate	$[m]$
y	Coordinate	$[m]$

Greek letters

α	Absorptivity or Absorbance	
β	Temperature volume expansion coeff.	$\left[K^{-1}\right]$
ϵ	Emissivity for radiation	
λ	wavelength	$[\mu m]$
μ	Dynamic viscosity	$\left[Nsm^{-2}\right]$
ν	Kinematic viscosity	$\left[m^2s^{-1}\right]$
ρ	Density	$\left[kgm^{-3}\right]$
ρ	Reflectivity or Reflectance	$\left[kgm^{-3}\right]$
σ	Stefan–Boltzmann constant	$\left[Wm^{-2}K^{-4}\right]$
τ	Transmissivity or Transmittance	

List of Figures

LIST OF FIGURES

List of Tables

Chapter 1

Introduction

1.1 The Kyoto Protocol

The *Kyoto Protocol to the United Nations Framework Convention on Climate Change (UNFCCC)* is an amendment to the international treaty on climate change, assigning mandatory emission limitations for the reduction of greenhouse gas emissions to the signatory nations. The objective of the protocol is the

> *stabilization of greenhouse gas concentrations in the atmosphere at a level that would prevent dangerous anthropogenic interference with the climate system* [1]

The text of the Protocol to the UNFCCC was adopted at the third session of the Conference of the Parties to the UNFCCC in Kyoto, Japan, on December 11^{th}, 1997; it was open for signature from March 16^{th}, 1998 to March 15^{th}, 1999 at United Nations Headquarters, New York. By that date the Protocol had received 84 signatures. Those Parties that have not yet signed the Kyoto Protocol may accede to it at any time.

The Protocol is subject to ratification, acceptance, approval or accession by Parties to the Convention. It entered into force on February 16^{th}, 2005 – the ninetieth day after at least 55 Parties to the Convention, incorporating Annex I Parties which accounted in total for at least 55% of the total carbon dioxide emissions for 1990 from that group, deposited their instruments of ratification, acceptance, approval or accession. 175 Parties have ratified the Protocol to date. Of these, 36 countries and the EEC are required to reduce greenhouse gas emissions below levels specified for each of them in the treaty. The individual targets for Annex I Parties are listed in the Kyoto Protocol Annex B. These add up to a total cut in greenhouse-gas emissions of at least 5% from 1990 levels in the commitment period 2008-2012.

At the moment only two different ways are possible in order to reduce the greenhouse gas emissions. The first is to use the less pollutant energy and

overall the renewable ones as well as hydroelectric, wind power, solar, etc. Otherwise the alternative is to reduce the energy consumption.

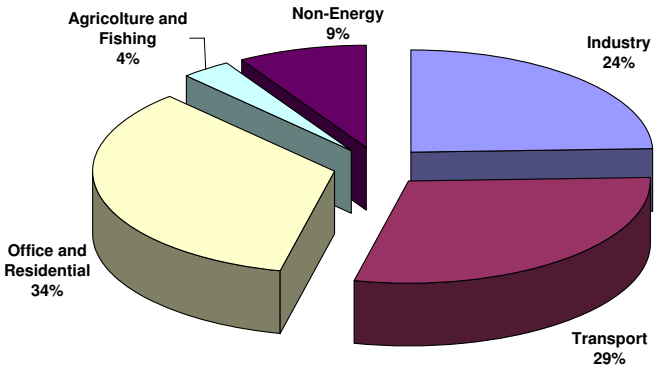

Figure 1.1: *World energy distribution*

As shown in Figure 1.1 (data from International Energy Agency, IEA[1]) a relevant part of the energy consumption is related to the extended meaning of the building construction compartment where construction costs and also maintenance, services, hygienic rules, security standard, thermal, acoustic and lightening comfort have to be included.

Different architectural energy saving technologies can reduce the energy leak and it is also possible to exploit the natural energy resources. In this sense smart systems in building shell assume a main importance in the global politics related to the greenhouse gas emissions reduction.

The international scientific community has taken up the challenge and the main world community involved in energy consumption developed research programs toward the smart systems in buildings facade. IEA has established an Implementing Agreement on Energy Conservation in Buildings and Community Systems (ECBCS)[2].

> *The function of ECBCS is to undertake research and provide an international focus for building energy efficiency. Tasks are undertaken through a series of annexes that are directed at energy saving technologies and activities that support their application in practice. Results are also used in the formulation of international and national energy conservation policies and standards.*

ECBCS undertakes the different related activities through specific Task Shared Annex and all the countries participates. The annex 44, in particular, based on the knowledge gained in the work so far (particularly the results of IEA Annexes 32, 35 and 37), will address the following objectives:

[1] `http://www.iea.org/`
[2] `http://www.ecbcs.org/`

- Define state–of–the–art of reactive building elements
- Improve and optimize reactive building elements and technologies
- Develop and optimize new building concepts with integration of reactive building elements, building services as well as natural and renewable energy strategies
- Develop tools for the early assessment of the impact of reactive building elements on the environmental performance of buildings
- Develop guidelines for procedures and tools for detailed simulation of environmental performance of reactive building elements and integrated building concepts

1.2 Buildings and environment

Heating, Ventilation, Air Conditioning (HVAC) technology provides several different solutions to reach environmental comfort but this is often traduced in a huge cost in terms of energy consumption. Energy saving in buildings is now a main objective for researchers.

The building energy balance is affected by the different thermo-physical phenomena generated by the interaction between the solar radiation and the different parts of the building itself. These components should be close linked by the unique aim to provide an improvement for the energy balance of the building.

Fenestration is one of the main subject concurring to the energy balance. Referring to [2] it is possible to define four basic mechanism: thermal heat transfer, solar heat gain, air leakage and daylighting. A strategy to minimize the energy effect of fenestration is also suggested:

1. using daylight to offset lighting requirements
2. using appropriate glazings and shading strategies to control solar heat gain to supplement heating through passive solar gain and and minimize cooling requirements
3. using appropriate glazings to minimize conductive heat loss
4. specifying low-air-leakage fenestration products

In addiction natural ventilation strategies can reduce energy use for cooling and fresh air requirements.

Double Skin Facade (DSF) works as a sort of *filter*. The facade has to be a barrier from the cold in winter or in cold location, but at the same time has to be an exhaust for the overheating in summer or in warm climate locations. The driving idea is to consider the facade of a building like a self adaptive one

in such a way that could change its behavior in the different environmental conditions.

The similitude with human being skin has been used from different authors to try to describe the concept. For example Lord Foster said[3]:

> *The envelope is the temperature control element – analogous to the human skin, it separates the interior from the exterior.*

Lord Rogers[4] also said:

> *A building becomes a chameleon which adapts. A properly equipped and responsively clothed building would monitor all internal and external variables, temperature, hygrometry and light levels, solar radiation etc., to determine the best energy equation given these conditions and modify the building and its internal systems accordingly. It is not too much to ask of a building to incorporate, in its fabric and its nervous system, the very basic vestiges of an adaptive capability*

1.3 Motivation and Objectives

Improvement of specific building elements is then one of the guidelines to positively influence the whole performances of a building. Following this statement building envelope represents a great contributor to the energy balance. Unfortunately there are still relatively few buildings in which DSF have been actually realized and till now it has not been possible to completely understand the real operating behavior. Furthermore the choice of the best typology should be led by the specific location and environmental conditions.

An experimental approach for the evaluation of DSF performances results in expensive test–campaigns and difficult measurements of important parameters. The definition of a mathematical model to simplify the real model, and its following solution, seems to be the most reliable and affordable approach. Thus different simplified methods have been developed from different researcher to calculate DSF performance (see section 1.4 for details).

The use of different heat transfer methods together with the fluid dynamics equations, could be a comprehensive suitable method to understand the functionality of the double facades. At the same time this approach represents a hard challenge due to the very complex thermo-fluid phenomena that characterize the DSF behavior under the different outdoor environmental conditions.

This work produces a comprehensive analysis to understand double–skin facades behavior using a *Computational Fluid Dynamics* (CFD) approach. This

[3] http://www.fosterandpartners.com
[4] http://www.richardrogers.co.uk

method allows a detailed analysis of the flow and thermal fields and the representation of the punctual value of every variable in the points of the modeled glazing system.

A step–by–step validation has been carried out during the research and finally experimental data kindly provided from Permasteelisa S.p.A. Research and Engineering Department have been used for the final confirmation of the effectiveness of the method.

This work would want to be preparatory to a following research and to the definition of a database for the development of an easy-to-use tool for designers that are approaching the problem without specific thermo–fluid dynamics knowledge.

1.4 State of the Art

As previously described there are still relatively few buildings in which DSF have actually been realized and consequently there is also too little experience about their operative behavior. Recently the importance of DSF in the global behavior of a test building have been analyzed in [3] using a software package for the thermal analysis of buildings. Different simplified methods are present in literature to calculate DSF performance or thermal exchanges such as nodal lumped variables procedures [4] or non-dimensional analysis [5]. The main part of the analysis are referred to the calculation of the overall heat transfer coefficient and a global energetic balance of the DSF.

The most complete approach to the problem is provided by the CFD, which supply comprehensive result for every single variable of interest. Basics information for indoor environment CFD analysis in order to define a standardized procedure for verification, validation and reporting is described in [6] and an example for procedure application is showed in [7]. Test about the ability of the CFD procedure and turbulence model to reproduce natural and mixed convection phenomena have been performed by [8], [9], [10] and many other.

The validation of a CFD code requires the comparison of the results with experimental data (see section 5). In the literature there is a significant lack of reliable experimental data and only few papers are devoted to the experimental analysis of the flow field in DSF.

In [11] an idealized representation of a real fenestration has been reproduced in laboratory to evaluate the influence of heated and turnable louvers on the convective heat transfer form an heated or cooled vertical isothermal surface. The results have been used to validate a two-dimensional CFD calculation. In [12] an experimental study on a full size single ventilated box window has been performed without shading devices varying the distance between the external and the internal facade.

In [13] the procedure used in [11] have been used to obtain detailed results about the effect of the heated louvers on the heat transfer rate from the surface. Convective heat transfer coefficients from an internal surface and adjacent

Venetian blinder have been examined in [14]. A simplified radiation method has been implemented in order to evaluate the diffuse radiation among the different part of the model. It has been found in recent literature that radiation models are difficult to implement, not user-friendly and mainly scarcely validated. An analysis of the influence of the blinder on the thermal performance of a double glazing window using a CFD procedure and involving a radiation model have been performed in [15].

A three-dimensional CFD analysis is provided in [16]. The study reviews energy interaction within double facade and key parameters affecting cavity width in design including the effect on functionally, practicality, aesthetics, cost and performances.

1.5 Overview of the Thesis

The main problem and the motivation for the thesis subject is introduced in Chapter 1 together with an analysis the most recent productions of the scientific community. The objectives of the work are also provided. A brief history and a classification of the DSF are also presented in Chapter 2.

An introduction to heat transfer basis related to indoor ventilation and DSF phenomena is provided in Chapter 3.

The link between CFD and indoor ventilation is introduced in Chapter 4, together a resume of the CFD procedure in thermo-fluid dynamics area.

In order to perform a simulation of a complex three–dimensional geometry validation of the CFD method is required. Test cases are presented in Chapter 5 to perform a step–by–step validation process. Well known analysis are reproduced and compared with high quality experimental and numerical results.

A full scale DFS has been reproduced and monitored by Permasteelisa R&E Department. Chapter 6 describes the experimental facility where experimental campaign has been made. Collected data useful for the purpose of this work has been provided and are presented here.

Finally, a comparison between experimental data, two–dimensional and three–dimensional predicted results are shown in Chapter 7. Critical analysis of the results is provided.

In Chapter 8 final conclusions are exposed and future work are planned.

Chapter 2

Double Skin Facades

2.1 Definitions

Different kind of fenestrations could be find in practical building. Referring to [2] a definition for **fenestration** is given:

> *Fenestration is an architectural term that refers to the arrangement, proportion, and design of window, skylight and door system within a building. Fenestration components include glazing material, either glass or plastic; framing, mullions, muntins, dividers, and opaque door slabs; external shading devices; internal shading devices; and integral (between-glass) shading system.*

A wide range of different type of fenestration products are available in commerce to meet the specifications for a project and a first rough distinction has to be made at first.

A criterion related to structural reasons [17] could lead to distinguish between *double windows* and *double facades* following different standard that address themselves specifically to windows, while others address themselves to facades.

A **Window** is defined as a component of the building intended to close a wall opening, permitting the passage of light and, possibly, ventilation. A **Facade** is defined as the exterior surface of a wall enclosing a building, usually non-loadbearing, which can include a curtain wall, cladding or other exterior finish. Finally a **Curtain Facade** is defined as a non-loadbearing wall positioned on the outside of the building and enclosing it [18].

DSF are essentially composed by two parallel glazing separated by a cavity; the whole became the vertical enclosure of a building. Each of these parallel glazing is commonly called a *skin* or a *layer*. The cavity enclosed between the two skins could have a vary different width length in the range from several centimeters to some meters according to the different facade type and could be ventilated or not.

In [19] a comprehensive literature review about the state–of–the–art related to DSF is described.

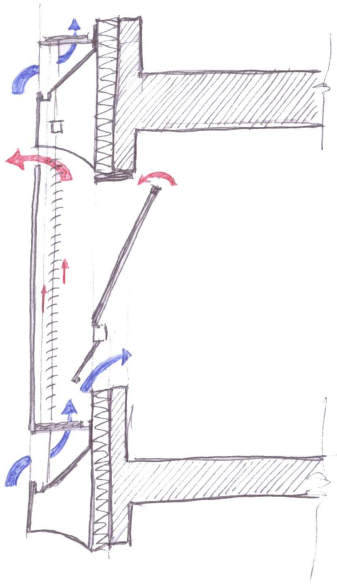

Figure 2.1: *Generic DSF scheme draft*

The Belgian Building Research Institute (BBRI) [20] defines:

> *An active facade is a facade covering one or several storeys constructed with multiple glazed skins. The skins can be air tighten or not. In this kind of facade, the air cavity situated between the skins is naturally or mechanically ventilated. The air cavity ventilation strategy may vary with the time. Devices and systems are generally integrated in order to improve the indoor climate with active or passive techniques. Most of the time such systems are managed in semi automatic way via control systems.*

BBRI includes also a description of the different components:

- Exterior glazing: usually it is a hardened single glazing. This exterior facade can be fully glazed.
- Interior Glazing: insulating double glazing unit (clear, lowE coating, solar control glazing, etc can be used). Almost always this layer is not completely glazed.
- The air cavity between the two panes. It can be totally natural, fan supported or mechanically ventilated. The width of the

cavity can vary as a function of the applied concept between 200 mm to more than 2 m. This width influences the way the facade is maintained.

- The interior window can be opened by the user. This may allow natural ventilation of the office.
- Automatically controlled solar shading system is integrated in the air cavity.

The cavity is connected with the outside air so that the windows of the interior facade can be opened, even in the case of tall buildings subject to wind pressures; this enables natural ventilation and night time cooling of the building's thermal mass. In winter the cavity forms a thermal buffer zone which reduces heat losses and enables passive thermal gain from solar radiation [21].

When solar radiation is high, the facade cavity has to be well ventilated, to prevent overheating. The key criteria are the width of the cavity and the size of the ventilation openings in the outer skin. The air change between the environment and the cavity is dependent on the wind pressure conditions on the building's skin, the stack effect and the discharge coefficient of the openings. These vents can either be left open all the time (passive systems), or opened by hand or by machine (active system) [21].

2.2 History

In [19] a brief history from DSF literature is described. Saelens [22] mentions that *in 1849, Jean-Baptiste Jobard, at that time director of the industrial Museum in Brussels, described an early version of a mechanically ventilated multiple skin facade. He mentions how in winter hot air should be circulated between two glazings, while in summer it should be cold air.*

Crespo, claims that, the first instance of a Double Skin Curtain Wall appears in 1903 in the Steiff Factory in Giengen, Germany. According to her, *the priorities were to maximize daylighting while taking into account the cold weather and the strong winds of the region. The solution was a three storey structure with a ground floor for storage space and two upper floors used for work areas. The building was a success and two additions were built in 1904 and 1908 with the same Double Skin system, but using timber instead of steel in the structure for budget reasons. All buildings are still in use.*

In 1903 Otto Wagner won the competition for the Post Office Savings Bank in Vienna in Austria. The building, built in two phases from 1904 to 1912 has a double skin skylight in the main hall.

At the end of the 1920s double skins were being developed with other priorities in mind. Two cases can be clearly identified. In Russia, Moisei Ginzburg experimented with double skin stripes in the communal housing blocks of his Narkomfin building (1928). Also Le Corbusieur was designing the Centrosoyus,

also in Moschow. A year later he would start the design for the Cite de Refuge (1929) and the Immeuble Clarte (1930) in Paris.

Little or no progress is made in double skin glass construction until the late 70s, early 80s. During 80s this type of facades they started gaining momentum. Most of these facades are designed using environmental concerns as an argument, like the offices of Leslie and Godwin. In other cases the aesthetic effect of the multiple layers of glass is the principal concern.

In the 90s two factors strongly influence the proliferation of double skin facades. The increasing environmental concerns start influencing architectural design both from a technical standpoint but also as a political influence that makes "green buildings" a good image for corporate architecture.

2.3 Classification

2.3.1 Classification by Ventilation System

The European Standard prEN 13119, specifying the terminology related with curtain walls, gives definitions for curtain walling and DSF [17]

> **Curtain Wall***: external building facade produced with framing made mainly of metal, timber or PVC-U, usually consisting of vertical and horizontal structural members, connected together and anchored to the supporting structure of the building, which provides, by itself or in conjunction with the building construction, all the normal functions of an external wall, but does not contribute to the load bearing characteristics of the building structure.*

> **Double Skin Facade***: a curtain wall construction comprising an outer skin of glass and an inner wall constructed as a curtain wall that together with the outer skin provide the full function of a wall.*

In the previous definitions, no reference is made about cavity ventilation, thus formally the term *Double Skin Facade* does not strictly designate a *ventilated* or *not ventilated* double facade.

The type of ventilation system could drive to a first classificatory criterion. Table 2.1[1] contains a classification of the DSF referring to the type of ventilation.

The Standard EN 12792 [23] defines **Natural Ventilation** as: *ventilation (...) which relies on pressure differences without the aid of powered air movement components.* The main forces that lead the precess are the difference of pressure created by the temperature gradient between inside and outside the cavity that drive to a stack effect and the effect of the wind. **Mechanical Ventilation** is defined as: *ventilation with the aid of powered air movement components.* **Hybrid Ventilation** is a sort of controlled ventilation where a

[1] *Hybrid* is the terminology coming from Permasteelisa s.p.a Company.

Table 2.1: *Name of the VDF concepts*

Type of Ventilation	Name of the facade concept
Natural	Passive facade
Mechanical	Active facade
Hybrid	Interactive facade

control system permits to shift between natural and mechanical ventilation via an automatic process based on an a control algorithm.

It is also important to highlight the relevance of the ventilation in DSF thermal performance. Kragh [24] specifies previous classifications according to the thermal conditions:

- **Naturally Ventilated Wall**: An extra skin is added to the outside of the building envelope. In periods with no solar radiation, the extra skin provides additional thermal insulation. In periods with solar irradiation, the skin is naturally ventilated from/to the outside by buoyancy (stack) effects - i.e. the air in the cavity rises when heated by the sun (the solar radiation must be absorbed by blinds in the cavity). Solar heat gains are reduced as the warm air is expelled to the outside. The temperature difference between the outside air and the heated air in the cavity must be significant for the system to work. Thus, this type of facade cannot be recommended for hot climates.
- **Active Wall**: An extra skin is applied to the inside of the building envelope; inside return air is passing through the cavity of the facade and returning to the ventilation system. In periods with solar radiation the energy, which is absorbed by the blinds, is removed by ventilation. In periods with heating loads, solar energy can be recovered by means of heat exchangers. Both during cold periods with no or little solar irradiation and during periods with solar gains or cooling loads, the surface temperature of the inner glass is kept close to room temperature, leading to increased occupant comfort in the perimeter zone, near the facade. This type of facade is recommended for cold climates, because of the increased comfort during the cold season and the possible recovery of solar energy.
- **Interactive Wall**: The principle of the interactive is much like that of the naturally ventilated wall with the significant difference that the ventilation is forced. This means that the

system works in situations with high ambient temperatures, as it does not depend on the stack effect alone. The system is thus ideal for hot climates with high cooling loads. During cold periods with no solar irradiation (e.g. during night-time) the ventilation can be minimized for increased thermal insulation. Apart from the advantages in terms of solar and thermal performance the system allows the use of operable windows for natural ventilation, even in highrise buildings.

2.3.2 Classification by Cavity Geometry

Another classification for DSF could be lead by cavity geometry considerations [19] [25] [22] [26]:

Figure 2.2: *Box Window (Mainz, DB Cargo Building) [25]*

- **Box Window**: horizontal and vertical partitioning divide the facade in smaller and independent boxes (Figure 2.2).
- **Shaft Box**: a set of box window elements are placed in the facade. These elements are connected via vertical shafts situated in the facade to ensure an increased stack effect (Figure 2.4)
- **Corridor Facade**: an horizontal partitioning is realized for acoustical, fire security or ventilation improvement. The cavity is accessible for easy maintenance(Figure 2.6).
- **Multi Storey Facade**: no horizontal or vertical partitioning between the two skins exists. Air cavity ventilation is provided via large openings near the floor and the roof of the building (Figure 2.8).

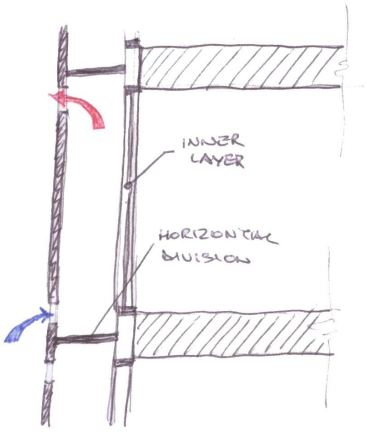

Figure 2.3: *Box Window ventilation scheme*

Figure 2.4: *Shaft Box (Dusseldorf, ARAG 2000 Tower) -* `http://gaia.lbl.gov/`

2.3.3 Classification by Ventilation Modes

The ventilation mode refers to the inlet origin and outlet destination of the circulating air inside the ventilated cavity and it is independent of the ventilation type as described in 2.3.1. Not all of the different ventilation modes can be applied in every facade type and of course a facade is characterized by only a single ventilation mode at time. Depending on the integration of certain technological component a single facade could work in different configurations in different specified situations.

It is possible to distinguish five different main ventilation modes [18]:

- **Air supply**: the ventilation of the cavity is created with outdoor air and this air is then used to supply the building.

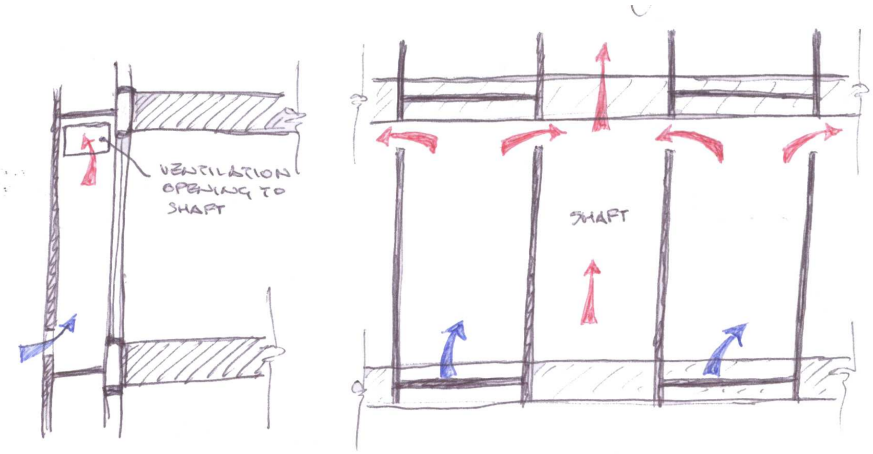

Figure 2.5: *Shaft Box Scheme*

Figure 2.6: *Corridor Facade (Dusseldorf, City Gate) -* `http://gaia.lbl.gov/`

- **Air exhaust**: the air comes from the inside of the building and is expelled toward the outside.
- **Outdoor curtain**: the air introduced into the cavity comes from outside and is immediately rejected toward the outside. The ventilation forms an air curtain enveloping the outside facade.
- **Indoor air curtain**: the air comes from inside of the room and it is returned to the inside of the room or via the ventilation system. The cavity forms an air curtain enveloping the indoor facade.
- **Buffer zone**: this ventilation mode is applicable to each of

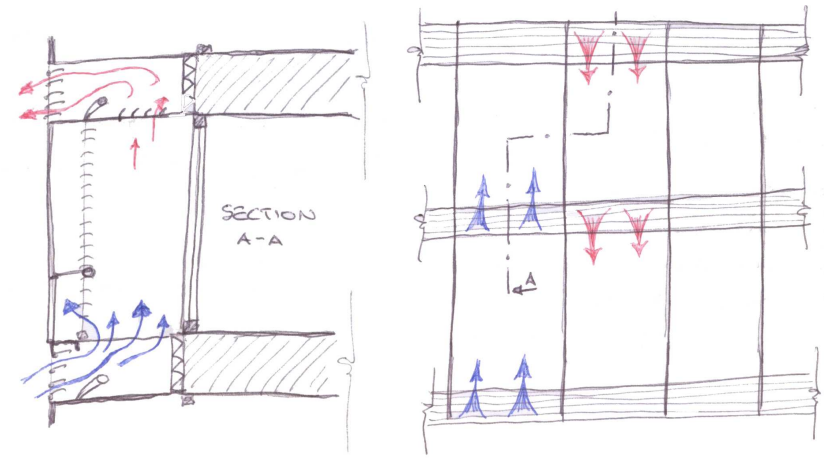

Figure 2.7: *Corridor Facade scheme*

Figure 2.8: *Multi Storey Facade (Cologne, Victoria Life Insurance Building) - http://gaia.lbl.gov/*

the double skin facades when they are made airtight. The cavity become a buffer zone between inside and outside and no ventilation being possible.

Motorized opening are often provided to naturally ventilated DSF in order to modify the ventilation mode in function of the different season conditions. Mechanically ventilated DSF are often not equipped to shift the ventilation mode so that most of time are characterized by a single mode.

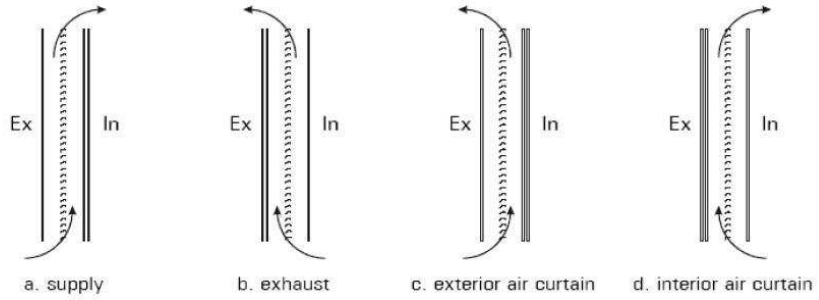

Figure 2.9: *DSF classification based on air flow [22]*

Chapter 3

Heat Transfer in Double Skin Facades

3.1 Introduction

A Double Skin Facade is subjected to very complex thermo-fluid phenomena under the outdoor environmental conditions, which involve conductive, convective, and radiative heat transfer with laminar, transient, and turbulent flow regimes. A propaedeutic theoretical analysis of the single aspects of the heat transfer fundamentals related to DSF needs to be provided.

According to [21] the complete structure of a building can be broken down into a hierarchy of substructures that define their different roles:

- Primary structure: Load-bearing core, columns, walls, floors and bracing required to carry horizontal and vertical loads.
- Secondary structure: Floors, which are not part of the primary system; built-in items, partitions, roof structures and annexes; facade elements.
- Tertiary structures: All constructions which are part of the secondary structures and whose stability is not critical to the stability of those secondary structures, e.g. a window within a facade element.

More detailed, the secondary structure can be divided into three main types [20]:

- Cantilever bracket structure
- Suspended structure
- Frame structure

The frame and the suspended structures are mainly involved in the thermal exchange of the whole facade. It is important to identify the parameters that influence the behavior of the DSF and to analyze how important the impact of these parameters is in order to actually understand if the use of this advanced facade could be suitable or not.

The air cavity can be used in several different ways as described in 2.3 according to the climatic condition, orientation, etc. The temperature of the air layer is influenced by many factors as described in [3]:

- Solar radiation level
- Orientation and shading devices use
- Opaque wall/window proportion of the interior facade
- Wind speed
- Color of shading device and of interior facade
- Depth of the double-skin cavity
- Glazing type in the interior facade
- Openings in the double skin

When the solar radiation strikes the the external skin of the facade it is partially reflected, absorbed and transmitted. The transmitted part into the cavity is the absorbed by the interior skin that warms up and in equilibrium conditions re-emits a long wave radiation in all the directions. When this radiations reaches again the external skin it is partially reflected and partially absorbed. The absorbed part is then re-emitted on both sides of the glazing. The result of this process is that a part of the original solar incident radiation is trapped inside the cavity causing an increase of the air temperature due of the convective heat exchange with the glazing wall. This process is known as **Greenhouse effect**.

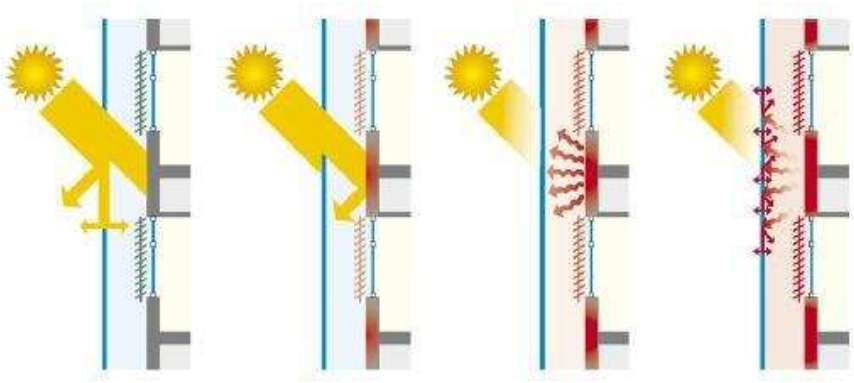

Figure 3.1: *Greenhouse effect in a DSF [27]*

Many glazing system have optical properties *spectrally selective* so that their properties vary across the electromagnetic spectrum and this is the main cause of the greenhouse effect. Glass is typically mainly transparent to the visible wavelength and mainly opaque for the long wave radiation.

When the sun is shining, especially in summer, the main factors that influence the DSF behavior are the orientation of the DSF and the heat produced as a result of absorption in the shading device [27] so it becomes very important to ensure an effective ventilation. In these conditions the stack effect (see 3.2.4) will dominate in natural ventilated DSF and the ventilation opening will be open during all day [27]. In Figure 3.2 a schematic solar energy distribution is shown.

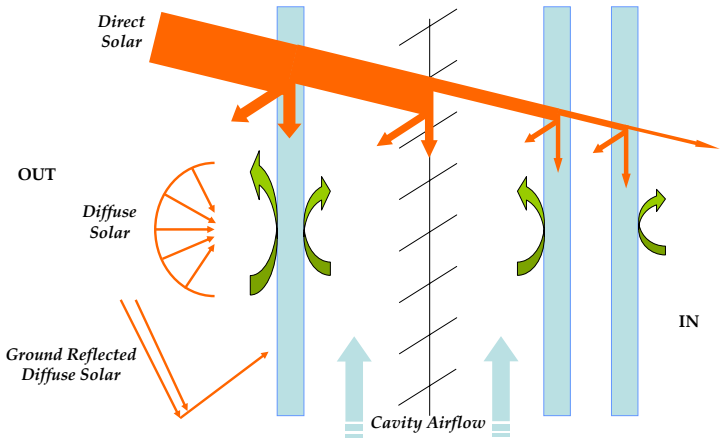

Figure 3.2: *Energy distribution in DSF with blinder device*

3.2 Heat transfer

3.2.1 Conduction

When inside a body a temperature difference is present heat flow will occur from the high temperature region to the low temperature region.

In glazing systems conduction occurs through the glass layer, the window frame and even the air or inert-gas fill in the cavity in double glazing windows. The conduction heat transfer rate is proportional to the temperature gradient as expressed by the *Fourier Law*:

$$q_k = -kA\frac{dT}{dx} \tag{3.1}$$

where the minus sign is a consequence of the second law of thermodynamics which require that heat transfer must occurs in the high to low temperature

direction. k in Equation 3.1 is the fluid *thermal conductivity* that indicate the amount of heat that will flow per unit time across a unit area when the temperature gradient is unity

3.2.2 Convection

Convection heat transfer occurs in window's glazing as shown in Figure 3.2. A flat heated plate cooled by an air flow is shown in Figure 3.3. It is interesting to notice how the velocity decrease in proximity of the surface. The flow region near the plate where the velocity of the fluid is decreased by viscous forces is called the **Boundary Layer**. The distance from the plate at which the velocity reaches 99% of the free stream velocity is arbitrarily designated as the boundary layer thickness and the region beyond this point is calle the indisturbed free stream [28].

In addition to the *momentum* boundary layer, a **Thermal Boundary Layer** will be present if a temperature difference exists between the solid surface and the fluid with which it is in contact (see Figure 3.3).

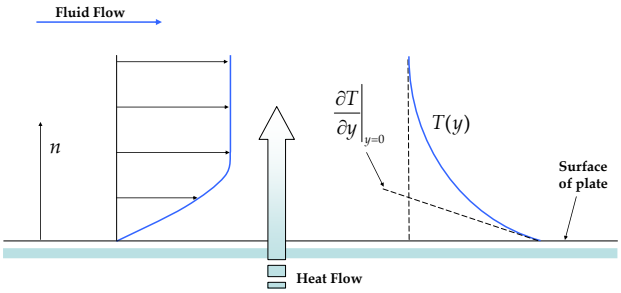

Figure 3.3: *Temperature and velocity distribution in a laminar forced convection flow over a flat plate*

If the velocity in the thin fluid layer close to the plate is zero then convective heat transfer occurs as described by:

$$q_c = -k_{fluid} A \left.\frac{\partial T}{\partial y}\right|_{y=0} \tag{3.2}$$

where q_c is the convection heat transfer ratio, k_{fluid} is the fluid thermal conductivity, A is the surface area, T are the plate and fluid temperatures and $\bar{h}_c$ is the averaged convective heat transfer coefficient. Though previous equation suggests a conductive heat transfer process, the surface thermal gradient is determined by the fluid energy transported in the main flow. The velocity field leads the wall temperature gradient, higher velocities produce higher temperature gradients. $\bar{h}_c$ depends on the surface geometry, the indisturbed fluid velocity, the physical fluid properties and the temperature difference. These

quantities are not necessary constant all over the whole surface so that it is possible to define a local coefficient and an averaged coefficient.

Irrespective of the detail of the mechanism, the rate of heat transfer by convection between a surface and a fluid can be calculated from the relation:

$$q_c = \bar{h}_c A \delta T \tag{3.3}$$

The relationship expressed by Equation 3.3 was originally proposed by the British scientist Isaac Newton.

This is quite similar in natural convection. In forced convection velocity tends to the undisturbed flow velocity value, in natural convection the velocity increase its value, as moving from the plate and reduce its value as density become similar to the fluid around. Buoyancy forces decrease as the fluid density value is near to the main flow value, so the velocity at first will rise till a maximum to decrease to zero value. The velocity field depends on the temperature difference between the fluid and the surface, the thermal expansion coefficient (that leads the density variation per temperature difference unit).

3.2.3 Non-dimensional Numbers

The solutions of the boundary layer equations for low-speed forced convection should be necessary to obtain the velocity and temperature profiles. In general these solutions are quite complicated so that different approach could be used to add considerable insight into the physical aspects of boundary layer flows as well as the form of similarity parameters governing the transport processes can be gained by non-dimensionalizing the governing equations. In convection heat transfer the key unknown is the heat transfer coefficient. Starting from Equation 3.2 it is possible to obtain an equation for h_c in terms of dimensionless parameters that suggests the appropriate form of the heat transfer coefficient called **Nusselt Number** [28].

$$Nu_L = \frac{h_c L}{k_f} \tag{3.4}$$

The parameters also represents the ratio of convection to conduction heat transfer in a fluid layer of thickness L. Dimensional analysis combined with experiments facilitates the understanding and extends the range of application of the experimental data by correlating them in terms of dimensionless groups. By using the *Buckingam* π *Theorem* and the *Principle of similarity*, it is possible to define important dimensionless number for the analysis of thermo fluid dynamics phenomena.

$$Re = \frac{\rho V L}{\mu} \tag{3.5}$$

is the **Reynolds Number** that represents the ratio of the inertial forces to the viscous forces and characterize the flow regime in a forced convection driven phenomenon.

$$Gr = \frac{g\beta\,(T_s - T_\infty)\,L^3}{\nu^2} \tag{3.6}$$

is the **Grashof Number** that represents the ratio of the buoyancy forces to the viscous forces and characterize the flow regime in a natural convection driven phenomenon.

$$Ra = \frac{C_p\rho^2 g\beta\,(T_s - T_\infty)\,L^3}{\mu k} \tag{3.7}$$

is the **Rayleigh Number** that could be written also as the product of the Grashof and Prandtl Number: $Ra = Gr\,Pr$. **The Prandtl Number** is expressed by:

$$Pr = \frac{c_p\mu}{\nu} \tag{3.8}$$

it is the ratio of the momentum diffusivity (viscosity) and it is a characteristic of the fluid.

3.2.4 Natural Convection

Wind and buoyancy due to the temperature gradient are the two forces which drive natural ventilation. In a building with DSF the temperature difference between the higher and lower ventilation openings become so important that the buoyancy due temperature gradient is dominant.

Natural ventilation phenomena in often commonly named as **Stack effect**. A volume of hot air will tend to rise in cold surrounding air. The relevance of this effect is influenced by the temperature difference between inside and outside air and by the height of the air column (stack).

DSF provides a good example of the occurrence of stack effect. The incident solar radiation increase the air temperature inside the cavity that become warmer than the external one. Because of the temperature variation a density variation occurs so that the air become lighter than the outside one. The air layer is in contact with the external and a pressure equalization process begin and the internal air will raise upward causing a state of excess pressure at the top where the heated air is ejected [27].

The air exchange between the environment and the cavity depends on the wind pressure conditions on the building's skin, the stack effect and the discharge coefficient of the openings [29].

For the simple system represented in Figure 3.4, the flowrate due to the stack effect is related to the temperature difference and is expressed by:

$$Q_v = C_d\,A\sqrt{g\,H\,\frac{\Delta T}{T_e}} \tag{3.9}$$

while the relationship between flowrate and pressure coefficient is given by:

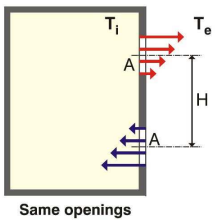

Figure 3.4: *Air flow generated by small openings [27]*

$$Q_v = C_d\, A \sqrt{\Delta C_p \frac{v^2}{2}} \tag{3.10}$$

where Q_v is the stack effect flow rate, C_d is the discharge coefficient, g the gravitational acceleration, h the height, ΔT the temperature difference between inside and outside, T_e the external temperature, v is the wind speed at the top and ΔC_p is the pressure coefficient difference between top and bottom.

3.2.5 Mixed convection

In any forced convection situation, some amount of natural convection is always present. When the natural convection is not negligible, such flows are typically referred to as mixed convection. The importance of the buoyancy forces in a mixed convection system could be defined through the **Archimedes Number** represented by the Grashof number and the square Reynolds number ratio:

$$Ar = \frac{Gr}{Re^2} = \frac{g\beta\,(T_s - T_\infty)\,L}{\nu^2} \tag{3.11}$$

When the ratio is near unity or higher, natural convection effects should not be neglected in a forced convection process. Otherwise in a natural convection process if the square Reynolds number is similar or higher respect of the Grashof number the forced convection influence become relevant.

3.3 Radiation

3.3.1 Theoretical fundamentals

Radiation allows heat to be transfered through wave energy commonly called *Electromagnetic Waves*, because energy travels in a combination of electrical and magnetic waves.

All the objects with a temperature above absolute zero emit radiation. As a consequence all normal real–life objects emit a wide range of radiation. Regardless of the type of radiation electromagnetic waves are propagated at the

speed of light ($3\times10^8\ m/s$) and it take places in the form of discrete quantum for which it is sometimes easier to assign them characteristics of pseudo-particles named *photons*.

The source of the electromagnetic radiation are vibrating electrons that are present in every atom that constitutes an object. The quantity of energy leaving a surface as radiant heat depends on the absolute temperature and the nature of the surface. A perfect radiator or *blackbody* emits radiant energy from its surface at a rate q_r given by the *Stephan-Boltzmann Law*:

$$E_b(T) = \frac{q_r}{A} = \sigma T^4 \tag{3.12}$$

where σ is a dimensional constant named *Stefan–Boltzmann Constant*:

$$\sigma = 5.67 \times 10^{-8} \left[\frac{W}{m^2 K^4}\right] \tag{3.13}$$

Following Equation 3.12 a blackbody surface with a temperature above of absolute zero radiates energy at a rate proportional to the fourth power of the absolute temperature. For engineering calculations involving real surfaces it is often important to know the energy radiated at a specified wavelength or in a finite band between specific wavelength λ_1 and λ_2 that is:

$$\int_{\lambda_1}^{\lambda_2} E_{b\lambda}(T) d\lambda \tag{3.14}$$

If a blackbody radiates in an enclosure that is also black, it will absorb all the radiant energy incident upon it, so the net radiant heat transfer is given by:

$$q_r = A_1 \sigma \left(T_1^4 - T_2^4\right) \tag{3.15}$$

where T_1 is the surface temperature and T_2 is the enclosure temperature. Of course real bodies does not meet the specifications of an ideal radiator but emit radiation with a lower rate than blackbodies. If they emit at the same temperature of the blackbody a constant fraction of blackbody emission at each wavelength, they are called *gray bodies*.

The emission of a blackbody at T_1 temperature inside a black enclosure at T_2 will be:

$$q_r = A_1 \epsilon_1 \sigma \left(T_1^4 - T_2^4\right) \tag{3.16}$$

where ϵ_1 is the *emissivity* of the gray surface and is equal to the ratio of the emission from the gray surface to the emission from a perfect radiator at the same temperature.

If both the two bodies are not perfect radiators it is necessary to introduce a dimensionless modulus that modifies the equation for perfect radiators to account for the emittance and relative geometries of the actual bodies.

$$q_r = A_1 \epsilon_1 \mathscr{F}_{1-2} \sigma \left(T_1^4 - T_2^4\right) \tag{3.17}$$

In most engineering calculations, total radiation properties as previously defined are sufficiently accurate [28]. When radiant energy is incident on a material surface, part of the radiation is:

- **Absorbed**: increasing the internal energy of the radiated object.
- **Reflected**: radiation is not absorbed or emitted from an object but it reaches the object and is sent backward.
- **Transmitted**: radiation is not absorbed, reflected, and it passes unchanged through the gas.

It is then possible to define the **reflectance** (or reflectivity) ρ as the fraction reflected, the **absorbance** (or absorptivity) α as the fraction absorbed and the **transmittance** (or transmissivity) τ as the fraction transmitted.

$$\rho + \alpha + \tau = 1 \tag{3.18}$$

If the angle of incidence is equal to the angle of reflection, the reflection is called *specular*. On the other hand, when an incident beam is distributed uniformly in all directions after reflection, the reflection is called *diffuse*.

Another important total radiation property of real surfaces is the **emissivity**. The emissive power of a body is defined as the energy emitted by the body per unit area and unit time. Now suppose that a body is placed inside an enclosure and allowed to come into temperature equilibrium with it. At equilibrium the energy absorbed by the body must be equal to the energy emitted if considering an ideal black body ($\epsilon_b = \alpha_b = 1$); otherwise there would be an energy flow into or out of the body which could rise or lower its temperature. The **emissivity** of a real surface (ϵ) is defined as the total radiation emitted divided by the total radiation that would be emitted by a blackbody at the same temperature:

$$\epsilon = \frac{E(T)}{E_b(T)} = \frac{E(T)}{\sigma T^4} \tag{3.19}$$

The energy balance on a monochromatic basis is:

$$\epsilon_\lambda + \rho_\lambda + \tau_\lambda = 1 \tag{3.20}$$

Under the condition that a body is in equilibrium with the surroundings it is possible to express the *Kirchoff Law* which states that the monochromatic emissivity is equal to the monochromatic absorbance for any surface.

$$\epsilon_\lambda(\lambda, T) = \alpha_\lambda(\lambda, T) \tag{3.21}$$

Although the above relation was derived under the condition that the body is in equilibrium with its surroundings, it actually a general relation that applies under any condition because both α_λ and ϵ_λ are surface properties that depend solely on the condition of the surface and its temperature.

Finally the *total hemispherical emittance* at a given temperature T for a non-black surface is:

$$\epsilon(T) = \frac{E(T)}{E_b(T)} = \frac{\int_0^\infty \epsilon(\lambda) E_{b\lambda}(\lambda, T) d\lambda}{\int_0^\infty E_{b\lambda}(\lambda, T) d\lambda} \tag{3.22}$$

A real surface radiation differs in several aspects form black–body or gray–body radiation. Any real surface radiates less than a blackbody at the same temperature. Gray surfaces radiates a constant faction ϵ_g of the monochromatic emissive power of a black surface at the same temperature T over the entire spectrum; real surfaces radiate a fraction ϵ_λ at any wavelength, but this fraction is non constant and varies with wavelength. Otherwise for wavelengths above $1.5\mu m$ the values of the gray–body emissive power fits fairly good the real surface trend. For temperature below $2000K$ the differences will not introduce a serious error because most of the radiant emission occurs at wavelength above $1.5\mu m$ [28].

3.3.2 Solar radiation

In passing through the earth's atmosphere, the sun's radiation is reflected, scattered, and absorbed by dust, gas molecules, ozone, water vapor, and water droplets (fog and clouds). The extent of this alteration at any given time is determined by atmospheric composition and length of the atmospheric path traversed by the sun's rays.

About half of the radiation is in the visible short-wave part of the electromagnetic spectrum. The other half is mostly in the near-infrared part, with some in the ultraviolet part of the spectrum.

Global solar radiation received by a surface is a combination of:

- Direct beam radiation I_b
- Sky or diffused radiation I_d
- Radiation reflected by the ground I_g

Thus it is possible to express the total irradiation reaching a terrestrial surface is the sum of the three above mentioned quantities:

$$I = I_b \cos\theta + I_s + I_g \tag{3.23}$$

As shown in figure 3.7 thermal radiation lies in the range from about $0.1\,\mu m$ and $100\,\mu m$, while the visible spectrum is very narrow about from $0.35\,\mu m$ and $0.75\,\mu m$.

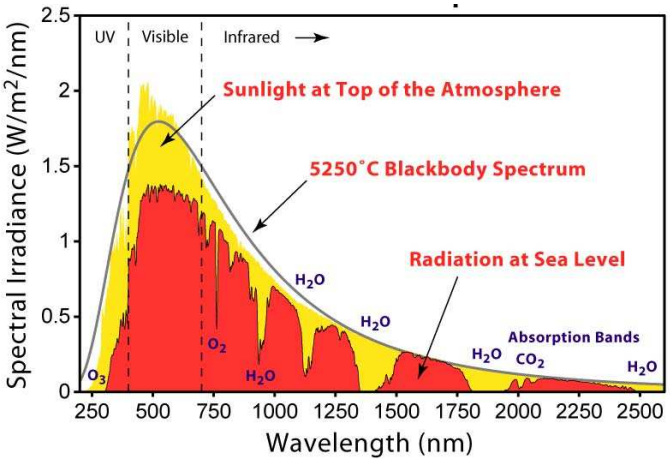

Figure 3.5: *Solar Spectrum – http://www.globalwarmingart.com/*

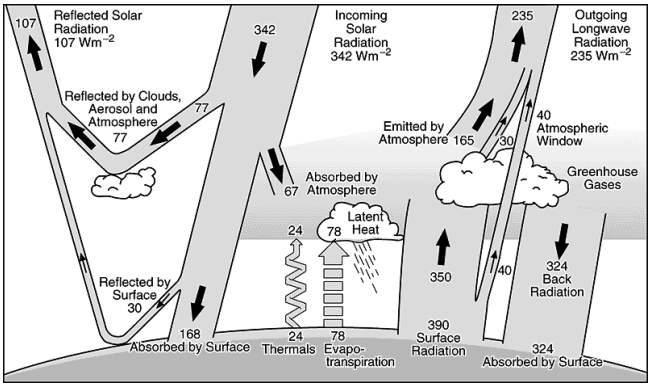

Figure 3.6: *The Earth's annual and global mean energy balance [30]*

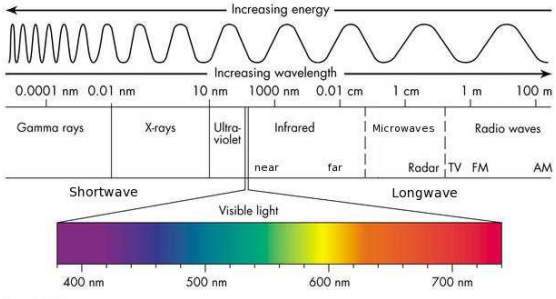

Figure 3.7: *Wavelength Spectrum - http://www.aos.wisc.edu/*

3.3.3 Instantaneous performance indices

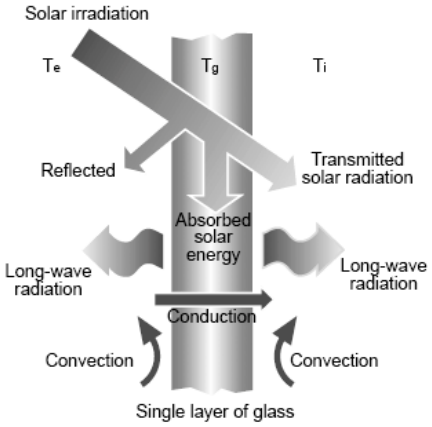

Figure 3.8: *Heat Transfer through a Single Pane of Glass [31]*

According to ASHRAE [2] energy flows through fenestration via conductive and convective heat transfer caused by the temperature difference between outdoor and indoor air, net long-wave (above 2500 nm) radiative exchange between the fenestration and its surrounding and between glazing layers, and short-wave (below 2500 nm) solar radiation incident on the fenestration product, either directly from the sun or reflected from the ground or adjacent objects. Simplified calculations are based on the observation that temperatures of the sky, ground, and surrounding objects (and hence their radiant emission) correlate with the exterior air temperature. The radiative interchanges are then approximated by assuming that all radiating surfaces (including the sky) are at the same temperature as the outdoor air. With this assumption, the basic equation for the instantaneous energy flow Q through a fenestration is:

$$q = UA_{pf}(t_{out} - t_{in}) + (SHGC)A_{pf}I \tag{3.24}$$

where q is the instantaneous energy flow, U the overall coefficient of heat transfer (U-factor), t_{in} the interior air temperature, t_{out} the exterior air temperature, A_{pf} the total projected area of fenestration, $SHGC$ the solar heat gain coefficient.

- **U-factor**: heat transmission in unit of time and through a unit of area. The lower U-fact is the greater is the window resistance to heat flow in addiction to a better insulation.
- **Solar Heat Gain Coefficient** (SHGC): the fraction of solar radiation admitted through a window on a skylight, both directly transmitted and absorbed and subsequently released

inside. The lower SHGC the less solar heat it transmit and the greater its shading ability.

- **Visible Transmittance** (VT) The fraction of visible radiation transmitted by a glazing system between the limits of 380-770 nanometers (more or less visible light). It is weighted according to the photopic response of the human eye (V-λ curve) and is expressed as a number between 0 and 1.

Chapter 4

CFD Approach

4.1 Introduction

Ventilation, as defined in [32], is the air used for providing acceptable and comfortable air indoor quality to minimize the potential for adverse health effects. Different pollution elements may affect the Indoor Air Quality (IAQ) such as microbial contaminant and chemicals (e.g. carbon dioxide from human breath) but also a high humidity or energy sources could reduce the comfort inside an indoor environment.

The ventilation control could be managed through a mechanical or forced system that produces a convenient air change. In order to reduce energy consumption natural ventilation is sometimes implemented to change the air in the indoor space without the use of a mechanical fans or exhausts. In many climates the natural ventilation process could not be sufficient to guarantee an optimal IAQ so that an air-conditioning system is often coupled.

The determination of the distribution of air velocity, temperature, contaminant concentration and thermal conditions become the actual first step to design an high-efficient air conditioning and ventilation system. As described in Chapter 6 the experimental measurements of the ventilation phenomena in a building or even in a room are normally difficult. Especially the measurement repeatability is almost impossible if referred to a real environment where the boundary conditions are continuously changing.

The physical phenomena are complicated by several concurring actions as described in [6]:

- Simultaneous heat flows (e.g., heat conduction through the building envelope, heat gains from object inside and solar radiation through fenestrations)
- Mechanical movements (e.g., fans and occupant movement)

The airflow, convective heat transfer and species dispersion are controlled

by the governing equation well known as Navier-Stokes Equations which can be expressed in the form:

$$\frac{\partial}{\partial t}(\rho\phi) + \frac{\partial}{\partial x_j}(\rho U_j \phi) = \frac{\partial}{\partial x_j}\left(\Gamma_\phi \frac{\partial \phi}{\partial x_j}\right) + S_\phi \tag{4.1}$$

Transient + Convection = Diffusion + Source

Numerical methods in industrial and scientific research have had large applications in the past 20 years thanks to the improvement of the computational power. The actual capability to transform a real world model into a mathematical model and then in a numerical model to simulate physical phenomena yields a flexible approach in most engineering applications.

The translation of this procedure into the fluid dynamics field brought to the development of a specific branch, the *Computational Fluid Dynamics* (CFD) that create proper codes to solve the governing equations of the specific phenomena.

The use of CFD methods in order to describe indoor ventilation is widely common in the scientific community and validation is often obtained with simplified test models, due to the practical difficulty to collect accurate data on real models.

The final objective of this research is to produce a background for the development of a simplified tool for constructor and designer of Double Skin Facades that permits a scientifically funded choice of the correct typology depending on the location and the climatic condition related to the actual place where the building has to be built.

Whatever could be the form of the tool, a software, a correlation or a table, a precise analysis of the behavior of the different operative conditions, typology and geometry should be carried out. In other words a parametric study has to be performed.

In chapter 2 has been shown that several typology of DSF may be considered depending on the ventilation type or geometry classification. In chapter 3 the parameters that influence the behavior have been identified and the variation in an opportune range should be considered to carry out a comprehensive tool.

It would be necessary for instance to consider the different types of ventilation, the ventilation rate, the depth of the cavity, the height of the facade section, the kind of a shading device, but also, in case of a Venetian Blinder, the different rotating position of the slats, etc.

It is easy to notice that a large number of different analysis would be necessary. If this should have been carried out experimentally, tens of experimental tests must be conducted. The experimental approach would be very expensive and time consuming. The use of a computational tool is the only alternative to the experimental parametric study.

Since DSF behavior is a very complex physical phenomena, both heat transfer and three–dimensional fluid dynamics problems are involved simultaneously.

In problems related to advanced windows, CFD is the most promising and full comprehensive modeling tool [33].

In this chapter a general review of the CFD approach will be provided.

4.2 CFD Procedure Introduction

The CFD code embeds the mathematical equations and directs the computer hardware to perform the calculations. Then the engineer inspects and interprets the computed results for the problem. Figure 4.1 illustrates the process.

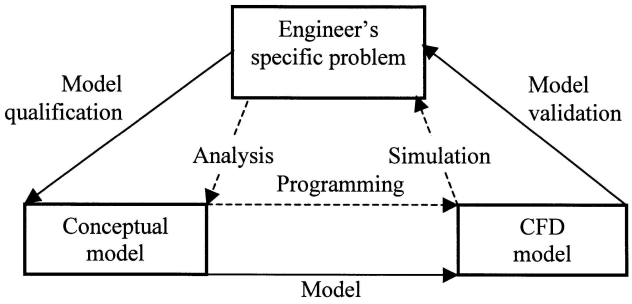

Figure 4.1: *Procedure for CFD modeling of an indoor environment and corresponding phase [6]*

According to [6] three fundamental steps are required to perform a reliable simulation:

- The **Verification** identifies the relevant physical phenomena for the indoor environmental analysis and provides a set of instructions on how to assess whether a particular CFD code has the capability to account for those physical phenomena.
- **Validation** provides a set of instructions on how to demonstrate the coupled ability of a user and a CFD code to accurately conduct representative indoor environmental simulations for which there are experimental data available.
- **Reporting of results** provides a set of instructions on how to summarize the results from a CFD simulation in such a way that others can make informed assessments of the value and quality of the CFD work.

Regarding the mathematical model, it is possible to directly solve the Navier-Stokes equations (4.1) for laminar flow cases and for turbulent flows

when all of the relevant length scales can be contained on the grid. This approach is called *Direct Numerical Simulation* (DNS). Unfortunately the computational cost of this approach is high if compared to most modern cluster machines capabilities that are not able to solve DNS in real scale problems.

In these cases, turbulent flow simulations require the introduction of a turbulence model. *Large Eddy Simulations* (LES) and the *Reynolds-averaged Navier-Stokes equations* (RANS) formulation (ref. to Par. 4.2.1) are two techniques for dealing with these scales.

In many instances, other equations (mostly convective–diffusion equations) are solved simultaneously with the Navier-Stokes equations. These other equations can include those describing species concentration, chemical reactions, heat transfer, etc. More advanced codes allow the simulation of more complex cases involving multi-phase flows (e.g., liquid/gas, solid/gas, liquid/solid) or non-Newtonian fluids (such as blood).

In all of the different approaches three are the basics steps to define and perform a CFD simulation:

- **Pre-processing**:
  - The geometry (*Model*) of the problem is defined.
  - The volume occupied by the fluid is divided into discrete cells (*Mesh*). The mesh may be structured or unstructured.
  - The numerical model (the governing equations) is defined
  - Boundary conditions are defined. This involves specifying the fluid behavior and properties at the boundaries of the problem. For transient problems, the initial conditions are also defined.
- The **Simulation** is started and the equations are solved iteratively as a steady-state or transient.
- **Post-processing**: a post-processor is used for the analysis and visualization of the resulting solution.

Numerical procedure on Navier-Stokes equations offers a very powerful and strong tool to predict velocity fields and heat transfer in fluid flows. CFD application in indoor environment, such as building rooms or airplane cabin, with natural and mixed convection phenomena, is currently one the most challenging subject with several application in both civil and mechanical engineering.

Analysis of air quality or environmental comfort are only some interesting facet of indoor environment modeling, in fact these aspects can be strongly linked with Heating and Ventilation Air Conditioning (HVAC) system and sustainable building design.

4.2.1 RANS Equations

The Navier-Stokes Equations (4.1) with the addiction of the state equation will be the mathematical tool for the solution of the mechanical energy part of a real physical phenomena. In turbulent flows the velocity field is characterized by fluctuating components that could be in very small scale and frequency. This could lead to a very long calculation time in order to solve the instantaneous equations.
Convenient mathematical manipulation may remove the small scales acting as a temporal or a spatial filter and noticeably reduce the calculation time. If a temporal filter is applied the terms can be decomposed in the fluctuant and mean part (*Reynolds decomposition*). Substituting in the momentum and continuity differential equations and imposing a temporal average the **Reynolds Averaged Navier-Stokes Equations** (RANS) are obtained:

$$\frac{\partial \rho}{\partial t} + \frac{\partial}{\partial x_i}\left(\rho u_i\right) = 0 \tag{4.2}$$

$$\begin{aligned} \frac{\partial}{\partial t}\left(\rho u_i\right) + \frac{\partial}{\partial x_j}\left(\rho u_i u_j\right) = \\ = -\frac{\partial p}{\partial x_i} + \frac{\partial}{\partial x_j}\left[\mu\left(\frac{\partial u_i}{\partial x_j} + \frac{\partial u_i}{\partial x_i} - \frac{2}{3}\delta_{ij}\frac{\partial u_i}{\partial x_i}\right)\right] + \frac{\partial}{\partial x_j}\left(-\rho\overline{u_i' u_j'}\right) \end{aligned} \tag{4.3}$$

The *Reynolds Stresses* $\left(-\rho\overline{u_i' u_j'}\right)$ are the additional unknown that have to be modeled in order to close the system. Unfortunately RANS equations, because of their general complexity (they are nonlinear, second-order, partial differential equations) are not amenable to exact mathematical solution except in a few instances. At the same way as before, the energy conservation equation can be expressed:

$$\begin{aligned} \frac{\partial}{\partial t}\left(\rho E\right) + \nabla \cdot \left(\bar{v}\left(\rho E + p\right)\right) = \\ = \nabla \cdot \left(k_{eff}\nabla T - \sum_j h_j \bar{J}_j + \left(\overline{\overline{\tau}}_{eff} \cdot \bar{v}\right)\right) + S_h \end{aligned} \tag{4.4}$$

where in the second term conduction, species diffusion and viscous dissipation terms can be found. In the Equation 4.4:

$$E = h - \frac{p}{\rho} + \frac{v^2}{2} \tag{4.5}$$

4.2.2 Using the solver

A **solver** as described in 4.2 will solve the governing integral equations for the conservation of mass and momentum, and (when appropriate) for energy

and other scalars such as turbulence and chemical species. A control-volume-based technique is used that consists of:

- Division of the domain into discrete control volumes using a computational grid
- Integration of the governing equations on the individual control volumes to construct algebraic equations for the discrete dependent variables (unknowns) such as velocities, pressure, temperature, and conserved scalars
- Linearization of the discretized equations and solution of the resultant linear equation system to yield updated values of the dependent variables

The *Segregated Solution Method* has been used in this work. The governing equations are solved sequentially and several iterations of the solution loop must be performed before a converged solution is obtained. A *Second Order Upwind Scheme* has been used for the discretization of the governing equations and the SIMPLE [34] pressure-velocity coupling algorithm. For more information refer to [35].

4.2.3 Turbulence model

Two equations eddy viscosity k-ϵ turbulence models are commonly adopted in indoor environment heat transfer calculations. Every single variation in this model formulation has been analyzed by Chen [8] in standardized natural, mixed and forced convection conditions.

Standard [36] and RNG k-ϵ [37] models resulted very stable during simulations but the ones run with standard model have been less accurate. In conclusion, RNG k-ϵ appear the most reliable and recommended turbulence model for indoor air flow simulations [8].

RNG k-ϵ model have been derived using a mathematical technical called *Renormalization Group* (RNG). Analytic formulation leads to different constants definition with additional terms and function in k and ϵ transport equations if compared with standard k-ϵ. The RNG k-ϵ model equations can be expressed:

$$\frac{\partial}{\partial t}(\rho k) + \frac{\partial}{\partial x_i}(\rho k u_i) = \frac{\partial}{\partial x_j}\left(\alpha_k \mu_{eff} \frac{\partial k}{\partial x_j}\right) + G_k + G_b - \rho\epsilon - Y_M + S_k \quad (4.6)$$

$$\begin{aligned} &\frac{\partial}{\partial t}(\rho\epsilon) + \frac{\partial}{\partial x_i}(\rho\epsilon u_i) = \\ &= \frac{\partial}{\partial x_j}\left(\alpha_\epsilon \mu_{eff} \frac{\partial \epsilon}{\partial x_j}\right) + C_{1\epsilon}\frac{\epsilon}{k}(G_k + C_{3\epsilon}G_b) - C_{2\epsilon}\rho\frac{\epsilon^2}{k} - R_\epsilon + S_\epsilon \end{aligned} \quad (4.7)$$

In these equations, G_k represents the generation of turbulent kinetic energy due to the mean velocity gradients. G_b is the generation of turbulence kinetic energy due to buoyancy. Y_M represents the contribution of the fluctuating dilatation in compressible turbulence to the overall dissipation rate. The quantities α_k and α_ϵ are the inverse effective Prandtl numbers for k and ϵ, respectively. S_k and S_ϵ are user-defined source terms.

Boussinesq Approximation for Density

The Boussinesq approximation (named for Joseph Valentin Boussinesq) is used in the field of buoyancy-driven flow. It states that density differences are sufficiently small to be neglected, except where they appear in terms multiplied by g, the acceleration due to gravity. The essence of the Boussinesq approximation is that the difference in inertia is negligible but gravity is sufficiently strong to make the specific weight appreciably different between the two fluids.

Boussinesq flows are common in nature (such as atmospheric fronts, oceanic circulation), industry (dense gas dispersion, fume cupboard ventilation), and the built environment (natural ventilation, central heating). The approximation is extremely accurate for many such flows, and makes the mathematics and physics simpler.

$$(\rho - \rho_o)\, g \cong -\rho_o \beta\, (T - T_o)\, g \tag{4.8}$$

In CFD this model treats density as a constant value in all solved equations, except for the buoyancy term in the momentum equation. Boussinesq approximation could get faster convergence than setting up a problem with fluid density as a function of temperature.

4.3 Radiation Modeling

While physical phenomena involving convection and conduction or both are simpler to model in a CFD environment, natural convection buoyancy-driven flows and especially radiation heat transfer are more complex [35]. The implementation of a radiation model should be necessary to accurately predict that situations where the radiant flux expressed by Equation 3.15 is large if compared to the heat transfer rate due to convection or conduction. Typically this occurs when high temperature are present and the fourth order dependence become dominant in the heat flux.

The **Radiative Transfer Equation** (RTE) [35] can be expressed for an absorbing, emitting and scattering medium:

$$\frac{dI(\vec{r},\vec{s})}{ds} + (a+\sigma_s) I(\vec{r},\vec{s}) = a\, n^2 \frac{\sigma T^4}{\pi} + \frac{\sigma_s}{4\pi} \int_0^{4\pi} I(\vec{r},\vec{s}\,')\, \Phi(\vec{s}\cdot\vec{s}\,')\, d\Omega' \tag{4.9}$$

where $\vec{r}$ is the position vector, $\vec{s}$ is the direction vector, $\vec{s}\,'$ is the scattering direction vector, s is the path length, a is the absorption coefficient, n is the refractive index, σ_s is the scattering coefficient, σ is the Stefan-Boltzmann constant, I is the radiation intensity, which depends on position ($\vec{r}$) and direction ($\vec{s}$), T is the local temperature, Φ is the phase function and Ω' is the solid angle.

The most reliable radiation model is probably the **Discrete Ordinates Model** [38], [39]. The DO model transforms Equation 4.9 into a transport equation for radiation intensity in the spatial coordinates (x, y, z). The DO model solves as many transport equations as there are directions $\vec{s}$. The solution method is identical to that used for the fluid flow and energy equations. A gray-band model is also implemented. For further information about DO model implementation in a solver software refer to [35].

Since radiation modeling of semi–transparent media is challenging, a decoupled method will be described and applied to take into account this form of heat transfer that strongly influences DSF thermo–fluid dynamics.

Chapter 5

Test Cases

5.1 Introduction to the Validation Process

Several physical phenomena have been analyzed to evaluate both the user and the software capability to accurately use the CFD tool. As the CFD modeling should provide a tool for design and analysis, an accurate validation process needs to be carried out. The strategy to perform a validation requires the identification of suitable experimental data in order to make sure that the main characteristics of the physical phenomena have been correctly modeled and also to define the uncertainty of the CFD calculation [6].

As mentioned in section 1.4 literature shows a significant lack of reliable experimental data about DSF and only few papers are devoted to the experimental analysis of the flow field.

Experimental data have been provided to validate the CFD prediction tool for the DSF (see section 6). Unfortunately indoor environment systems are usually complicated and experimental data may also contain biased and random error [6] then a step–by–step process validation with data from the literature has been performed as well.

Some classical cases with high quality experimental data have been analyzed to reproduce step–by–step the different phenomena that may occur in DSF operative behavior. Four among the studied cases are presented in this chapter, starting from the classical square cavity. To demonstrate the ability to predict a natural convection phenomena in a narrow cavity, the case presented in section 5.3 and a two–dimensional enclosed cavity with high aspect ratio have been modeled. Then a complete indoor environment problem will be described in 5.2 consisting in a simplified office room simulated in order to reproduce the ventilation and temperature behavior (see 5.4). Finally a simplified test window facade with adjacent Venetian blinder will be presented in 5.5 before to go directly to the main subject of this work in the next chapter.

5.2 Square Cavity

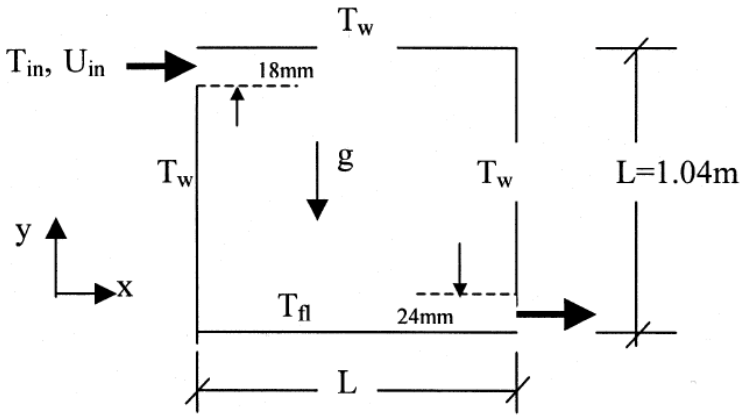

Figure 5.1: *Geometrical Model*

This test case has been used for verify the ability of the CFD code to predict mixed convection. The experiment maintained a temperature, $T_w = 15^oC$, at the two vertical walls and the top wall, while the floor was heated to a higher temperature, $T_{fl} = 35.5^oC$. An air jet with a temperature of 15^oC was discharged horizontally into the cavity at a velocity that varied from $0.25m/s$ to $0.57m/s$. The Reynolds number is 658 based on the inlet height or 38000 based on the cavity height. The Rayleigh number is 1.8×10^6.

The domain has been discretized through a Cartesian orthogonal grid and a near wall grading has been used in order to directly solve both the fluid dynamic and the thermal boundary layer. The Cartesian coordinates and structured mesh produce a faster convergence with the finite-volume method. According to [8] the computational mesh used during calculations, see Figure 5.3, has been built in order to obtain a $y^+ \cong 10$ value, suitable for an indoor ventilation displacement simulation.

The non-dimensional wall distance y^+ is defined as:

$$y^+ = \frac{u_* y}{\nu} \tag{5.1}$$

where u_* is the friction velocity at the nearest wall, y is the distance to the nearest wall and ν is the kinematic viscosity of the fluid.
The upwind SIMPLE scheme has been used to perform calculations.

The flow pattern of the flow field in the cavity has been reconstructed and compared with the predicted velocity field as shown in Figure 5.2. Predicted values for velocity and temperature have been compared with punctual probe measurements.

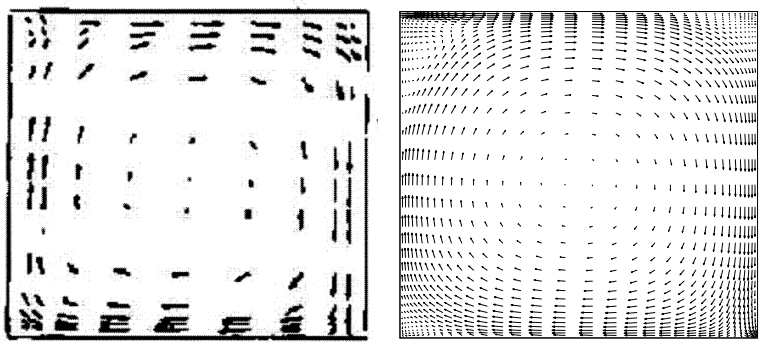

Figure 5.2: *Flow Patterns experimental and predicted data comparison*

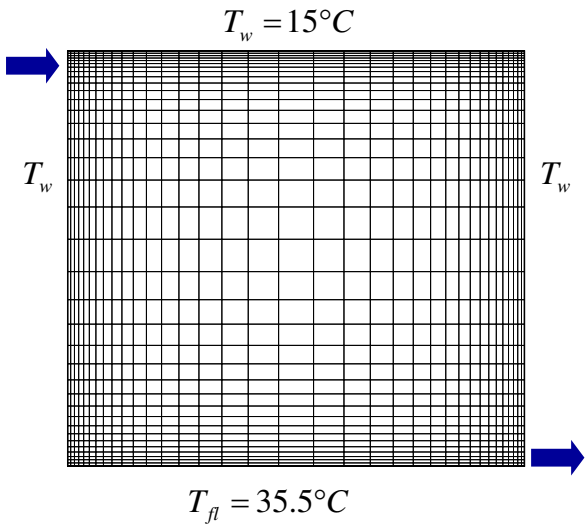

Figure 5.3: *Computational model and structured grid*

Velocity profile predicted values follow almost perfectly the measure values as shown in Figure 5.4 and also the boundary layer trend close to the cavity wall fits very closely. Thermal boundary layer and the general temperature profile are in close agreement with the experimental results as shown in Figure 5.5.

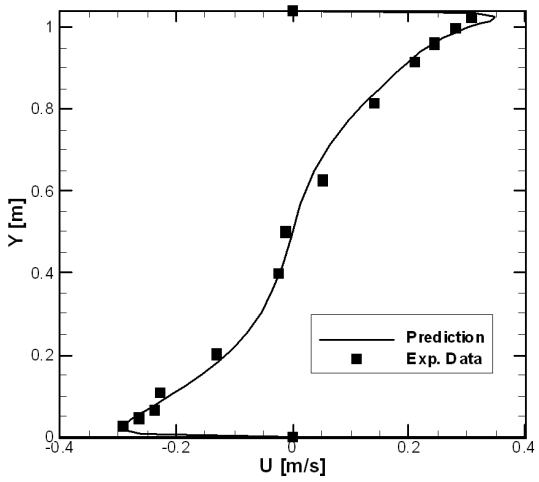

Figure 5.4: *Velocity profile at* $x/W = 0.5$

An overall analysis shows that the predicted results are in close agreement with the experimental data and how it is possible to simulate with very good precision the mixed convection phenomena.

5.3 Tall Enclosed Cavity

A two–dimensional enclosed cavity with high aspect–ratio and natural convection phenomena has been analyzed. Experimental data for this case have been presented in [40].

A steady–state simulation has been performed. Turbulence has been modeled using the RNG k–ϵ model and Boussinesq approximation has been set for density modeling. Adiabatic and non–slip condition have been used as boundary condition for the top and bottom walls, and constant temperature have been used for right and left walls. A temperature difference has been also set between left and right walls and two cases have been analyzed. Table 5.1 describes a summary of the boundary conditions for Case1 and Case2.

The exact hot and cold temperatures were not reported in [40]. Nevertheless temperature difference is the governing force in buoyancy driven flow and, since the considered fluid is air, a variation of the wall temperature while keeping

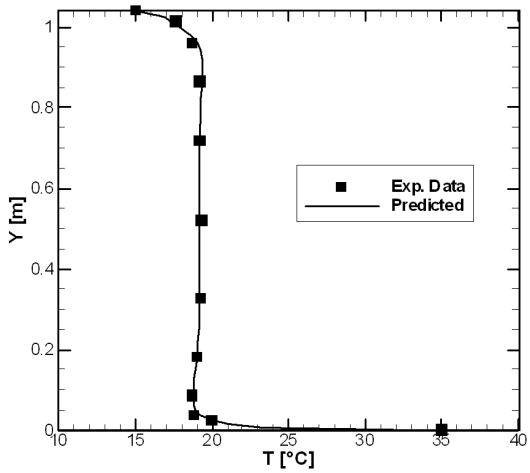

Figure 5.5: *Temperature profile at* $x/W = 0.5$

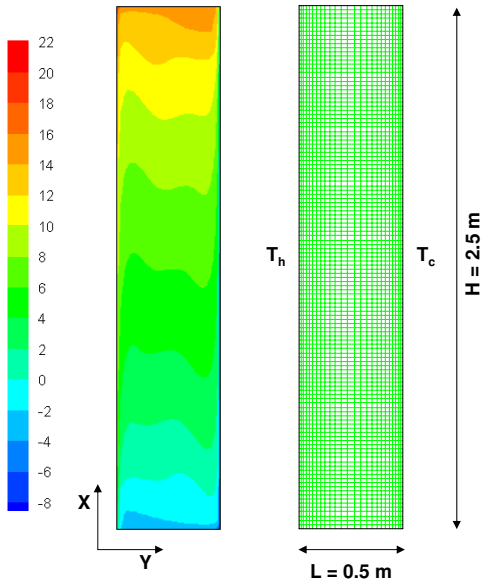

Figure 5.6: *Geometrical Model with non–uniform mesh (left). Temperature contour for Case2 (right)*

Table 5.1: *Boundary conditions for Case1 and Case2*

	T_h (^oC)	T_h (^oC)	δT (^oC)
Case1	35.8	-10	45.8
Case2	22.1	-10	32.1

constant the temperature difference would not mainly affect the airflow patterns [41]. Of course this is true in normal indoor environment were temperature range are small and air properties vary little. For Case1 the Rayleigh number is 4.25×10^{10}, and for Case2 is 2.84×10^{10}.

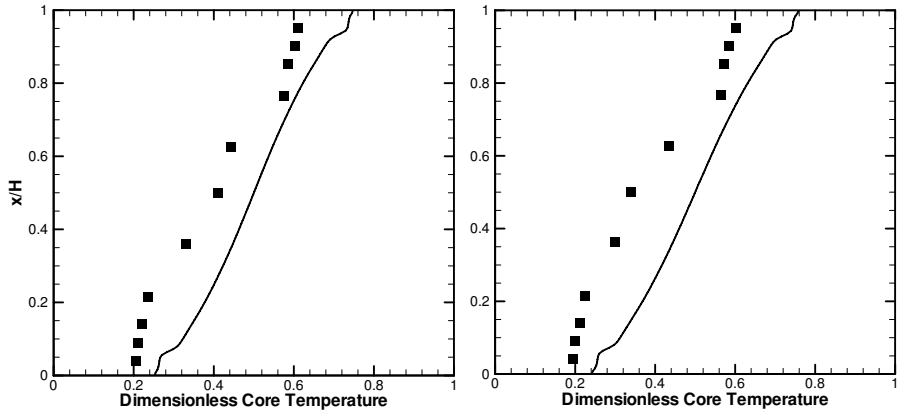

Figure 5.7: *Results comparison: Core Temperature – Case1 (left) and Case2 (right) – ■: experimental data; —: predicted values.*

Figure 5.7 shows the comparison between non–dimensional predicted core temperature θ measured on a vertical middle–span line and those reported in [40]. Non–dimensional core temperature was defined as

$$\theta = \frac{T - T_c}{T_h - T_c} \tag{5.2}$$

Predicted data well fit the experimental results both in Case1 and Case2. In Figure 5.8 the velocity profile calculated on an horizontal line at middle–height is shown.

It is interesting to notice that the velocity profile shows a typical natural convection behavior where, due to the temperature gradient, velocity first increases its value moving from the hot wall and then reduces its values when temperature decreases approaching the core temperature. As expected velocity

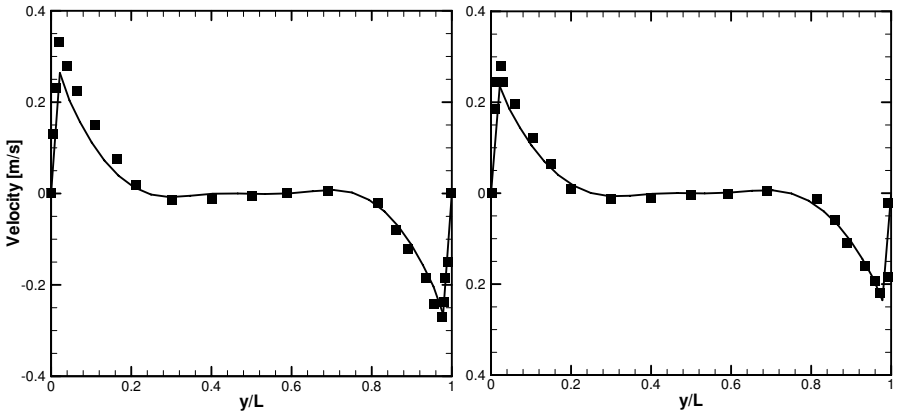

Figure 5.8: *Results comparison: Velocity profile at middle height – Case1 (left) and Case2 (right) – ■: experimental data; —: predicted values.*

magnitude is positive on the hot wall side and negative on the cold wall side and the profile appears almost symmetric due to the geometry configuration. Data comparison shows a good agreement with experimental values.

5.4 Office Room

A complete indoor environment system has been simulated according to [7]. Displacement ventilation in an office has been simulated using the configuration shown in Figure 5.9. One supply diffuser, one exhaust, two computers, two tables, two boxes, and six lamps are the room furniture and two occupants are included in the office.

The main part of the object that are present in the room are rectangular, but although some are not, e.g. the occupants, it is not necessary to reproduce the real geometry of a human body or to use a non-structured mesh because the contribution of the body-shape to the airflow is negligible. Thus a Cartesian structured mesh has been used.

The radiative heat from the heated objects could be calculated with Equation 3.15, where in this case 1 is related to the object and 2 is related to the walls. The surface temperature of the heated objects has to be estimated based on user's experience and uncertainties are introduced. The convective heat is thus calculated as the total heat (see Table 5.2) minus the radiative heat. The convective heat is then assumed to be uniform distributed on the object surface [7].

In this test case, all the wall temperatures were prescribed, but in a real room are actually unknown. It could be possible to estimate the wall surfaces temperature through an energy simulation program or a conjugate heat transfer

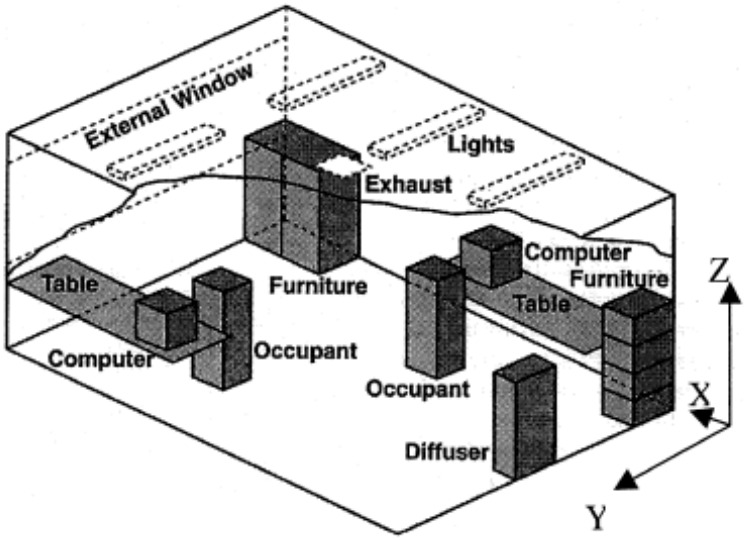

Figure 5.9: *Geometrical Model*

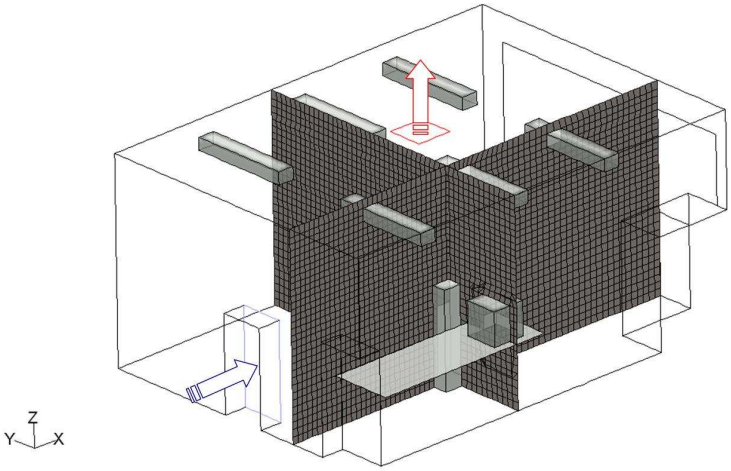

Figure 5.10: *Model discretization*

Table 5.2: *Detailed thermal boundary conditions for the heated objects in the office. The heat generated includes radiation and convection and the effective area ratio of the diffuser is 10%*

Item	Length	Width	Height	Location			Heat
	$\Delta x\,[m]$	$\Delta y\,[m]$	$\Delta z\,[m]$	$x\,[m]$	$y\,[m]$	$z\,[m]$	$Q\,[W]$
Room	5.16	3.65	2.43	0.0	0.0	0.0	
Window	0.02	3.35	1.16	5.16	0.15	0.94	
Diffuser	0.28	0.53	1.11	0.0	1.51	0.03	
Exhaust	0.43	0.43	0.0	2.365	1.61	2.43	
Occupant 1	0.4	0.35	1.1	1.98	0.85	0.0	75
Occupant 2	0.4	0.35	1.1	3.13	2.45	0.0	75
Computer 1	0.4	0.4	0.4	1.98	0.1	0.75	108.5
Computer 2	0.4	0.4	0.4	3.13	3.15	0.75	173.4
Table 1	2.23	0.75	0.01	0.35	0.0	0.74	0.0
Table 2	2.23	0.75	0.01	2.93	2.90	0.74	0.0
Box 1	0.33	0.58	1.32	0.0	0.0	0.0	0.0
Box 2	0.95	0.58	1.24	4.21	0.0	0.0	0.0
Lamp 1	0.2	1.2	0.15	1.03	0.16	2.18	34
Lamp 2	0.2	1.2	0.15	2.33	0.16	2.18	34
Lamp 3	0.2	1.2	0.15	3.61	0.16	2.18	34
Lamp 4	0.2	1.2	0.15	1.03	2.29	2.18	34
Lamp 5	0.2	1.2	0.15	2.33	2.29	2.18	34
Lamp 6	0.2	1.2	0.15	3.61	2.29	2.18	34

model even though further validation of the CFD simulation may be needed, and there may not be suitable experimental data for this additional validation.

In figure 5.11 and in Figure 5.12 qualitative representation of the flow and temperature fields inside the room are shown. The predicted air flow pattern is compared with measured data and the trend is in close agreement.

Experimental data in different positions of the room has been monitored during experiments. For brevity only middle room line result comparison in correspondence of the exhaust will be represented. Figure 5.13 shows both the velocity and the temperature profile. If compared with experimental data, predicted results has a good agreement.

In Figure 5.14 is shown the center–line turbulent kinetic energy profile. Even if this second order characteristic of th fluid flow is normally difficult to simulate, the predicted values well fit experimental data.

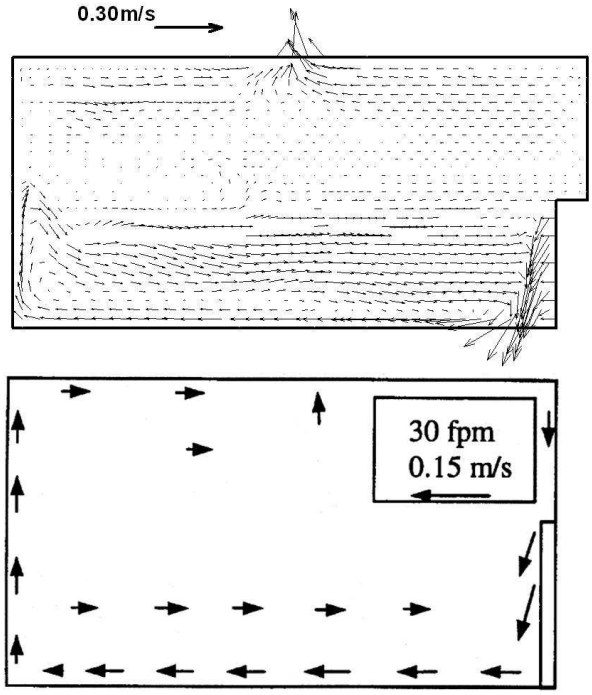

Figure 5.11: *Air flow pattern comparison in the mid section*

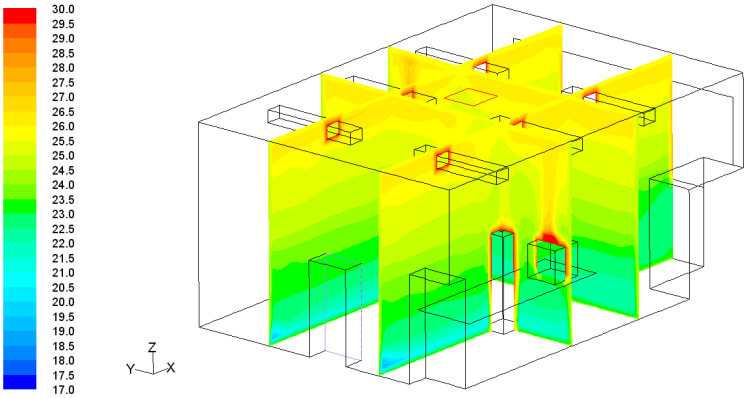

Figure 5.12: *Temperature distribution*

As a conclusion it seems possible to affirm that mixed convection phenomenon and complete indoor environment problem have been simulated with very good results. Next step is directed to approach the main objective of this work and a laboratory model of a window with a shading device will be analyzed and simulated.

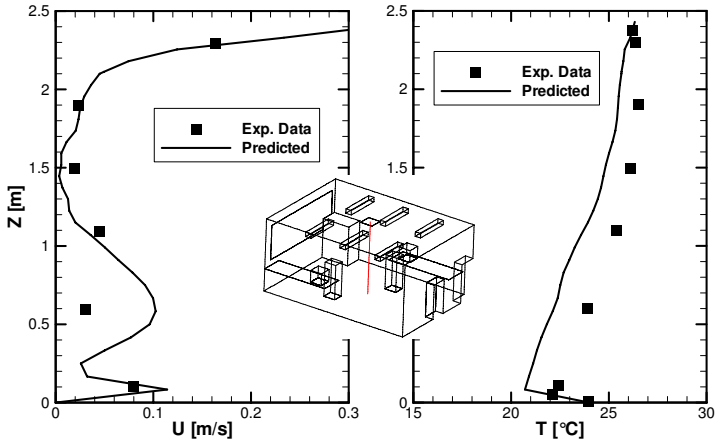

Figure 5.13: *Center-room vertical line Temperature and Velocity profile*

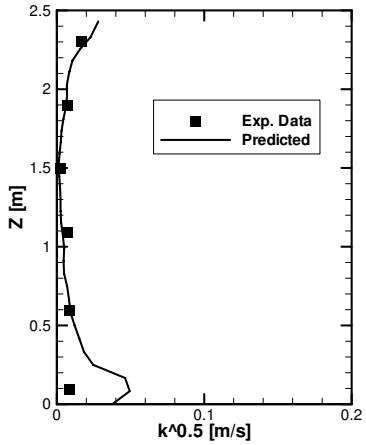

Figure 5.14: *Center-room vertical line Turbulent Kinetic Energy profile*

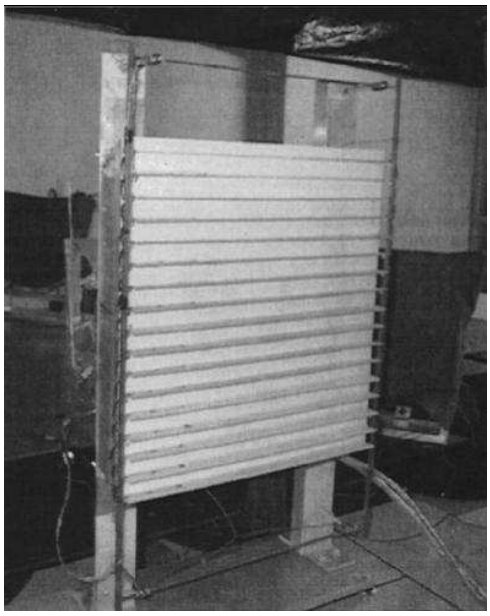

Figure 5.15: *Picture of experimental setup [14]*

5.5 Laboratory Window Model

In DSF configuration is quite usual to have a louvered shading device, such as a Venetian blind, mounted alternatively on the outdoor or the indoor surface or inside the ventilated cavity to provide privacy and to control day-lighting. Moreover the presence of the shading devices affect the natural convection and radiant heat exchange in the window system. As a result, there will be a change in the heat transmission and solar heat gain.

Different authors have studied the behavior of a shaded window. In [42] a numerical simulation including heat conduction along the blind slats and radiation heat exchange has been performed. In [11] and [14] presented a detailed validation and numerical analysis as described in Section 1.4. Convective heat transfer coefficients from an internal surface and adjacent Venetian blinder have been examined in [14].

To be confident in the analysis of physical problems including Venetian blinder influence, some results presented in [14] have been reproduced. The experimental setup is shown in Figure 5.15 and have idealized the indoor glazing surface as an isothermal vertical flat heated surface. On the internal side it has been positioned a shading device composed by 17 slats.

Simulations have been referred to the case where the Reynolds number calculated on blind pitch spacing has been set to 10000.

The ambient room temperature where have been set to $T_i = 293.0K$, the

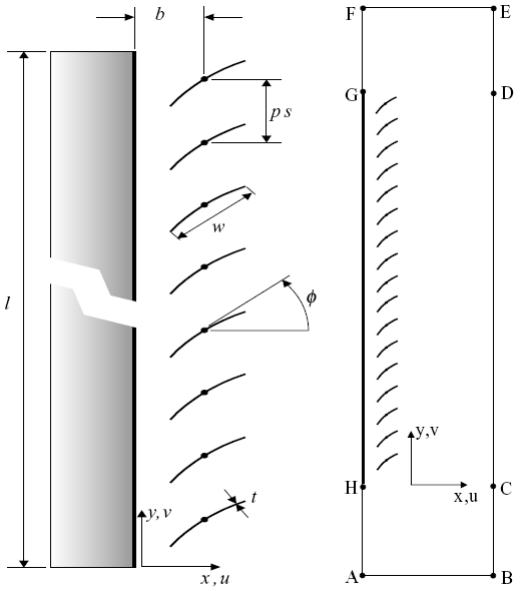

Figure 5.16: *Scheme of the numerical model [14]*

isothermal vertical heated flat surface temperature to $T_g = 302.6K$. A temperature T_b has been applied to each slat to simulate the solar radiation absorbed and re–emitted by the Venetian blinder $T_b = 307.4K$. The nominal blind spacing was $b = 25.4mm$ and the blind slat angle $\Phi = 0^o$. Figure 5.16 shows the system geometry.

The dimensionless boundary conditions referring to Figure 5.16 are:

$$\begin{aligned} U = V = 0 \qquad & \theta_g = 1 && (GH) \\ U = V = 0 \qquad & \theta = 1 && (FG, HA) \\ \frac{\partial U}{\partial X} = V = 0 \qquad & \theta_i = 0 && (BCDE) \end{aligned}$$

where U and V represent the dimensionless velocity and θ the dimensionless temperature. For a detailed explanation of these terms please refer to [14]. No-slip condition has been applied at the surface of the slats.

During steady-state simulations the fluid has been considered as an incompressible ideal gas and the flow has been modeled two-dimensional, and the regime has been laminar. The thermo-physical properties has been set constant, except for fluid density where Boussinesq approximation has been used (see sec. 4.2.3).

In Figure 5.17 a comparison of the predicted isothermal with the observed is shown. In Figure 5.18 a comparison of the streamline plot is made. Although

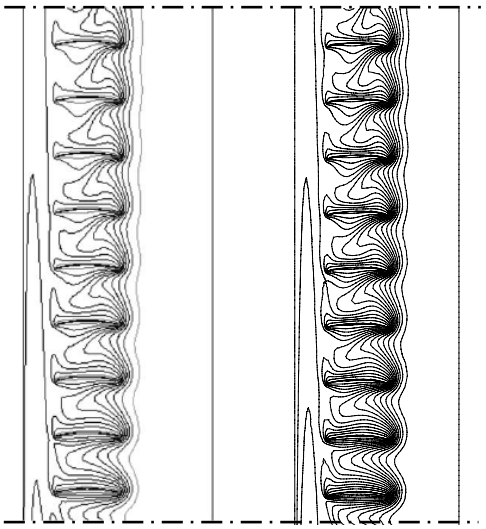

Figure 5.17: *Paper and predicted iso-therm comparison*

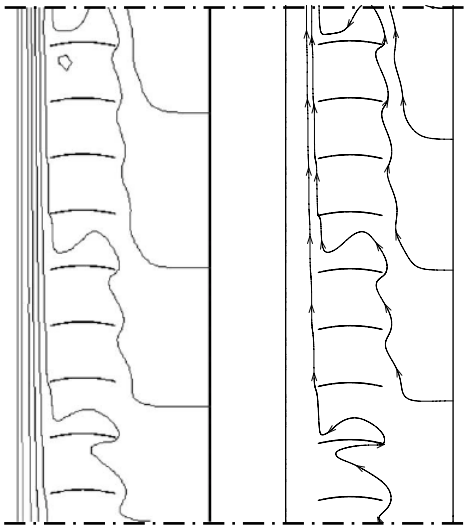

Figure 5.18: *Paper and predicted stream-function comparison*

no quantitative information could have not been compared, the trend is in almost perfect agreement with the reference paper both for streamlines and temperature.

5.6 Conclusion

The test cases presented in this chapter demonstrate the ability of the CFD code to simulate the indoor ventilation phenomena with very good approximation.

Part of the path that has led to the main subject of this thesis has been presented. Starting from a classical case of mixed ventilation in a cavity, some examples with added complexity have been solved. Finally a test case with a good level of similarity respect to the final objective has been reproduced.

In all of proposed cases comparison of the CFD results with with literature data shows a close agreement. Both the temperature and the velocity field are well resolved and also the thermal and and flow boundary layer are well reproduced.

A grid sensitivity study confirms the near–to–wall cell size proposed in [8], together with the convenient mesh density in the internal part of the computational domain.

These results will be used for the simulation of a complete commercial mechanically ventilated DSF and validation of the results will be proposed that will be presented in the next chapter.

Chapter 6

Full Scale Double Skin Facade Experimental Data

6.1 Introduction

The validation process of a CFD procedure needs a comparison of the predicted results with experimental data or numerical results of declared accuracy. A step–by–step validation procedure of this kind has already been performed in chapter 5 for test cases concerning internal flow in simple cavities or complex building rooms.

Figure 6.1: *Permasteelisa Campus* - `http://www.permasteelisa.com`

For the actual subject of this work (i.e. DSF analysis) scientific literature presents a lack of experimental data, as previously mentioned. Only simplified

models of window have been studied in laboratory, and the few full scale tests are generally used for the calculation of the overall heat transfer coefficient and of the global energetic balance of the DSF (see sec. 1.4). In general few experimental data related to flow fields and temperature are available. This lack may be justified by noticing that environment system measurements are difficult to carry out and subjected to high biased and random error.

To provide a comparison of the CFD results with experimental data collected for DSF system, a collaboration deal with the Permasteelisa S.p.A., R&E Department, has been started. Permasteelisa is a multinational company specialized in the production of glazing envelopes. Permasteelisa experimental campus, located in San Vendemiano, Treviso, Italy (Figure 6.1), is equipped with full scale test rooms where different type of glazing facade can be testes and monitored in terms of both energetic consumption and internal environmental conditions.

An internal report [43] about an advanced DSF measurement campaign has been released in 2002 and experimental data have been kindly provided by the company to D.I.Me.Ca. for the purpose of this work. The report is referred to the Test Room n. 5 equipped with an instrumented and monitored advanced Double Skin Facade with integrated Venetian blinder in the ventilated cavity, named Interactive Wall. Different configuration of the facade have been tested, for varying environmental condition.

6.2 Experimental Setup

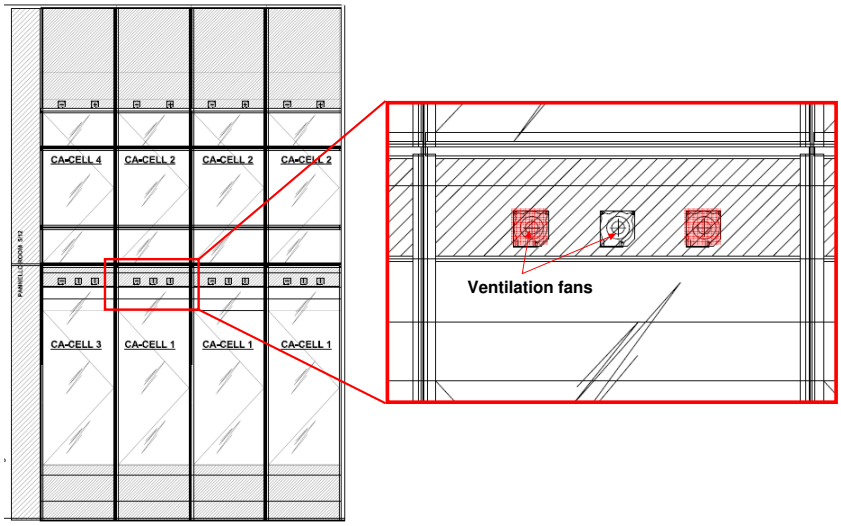

Figure 6.2: *Permasteelisa DSF*

FULL SCALE DOUBLE SKIN FACADE EXPERIMENTAL DATA

Front and side views together with the geometrical configuration of the studied DSF are reproduced in Figure 6.2 and Figure 6.3 For the sake of clarity only the top part of the facade at the ground floor and the bottom part at the upper floor are shown.

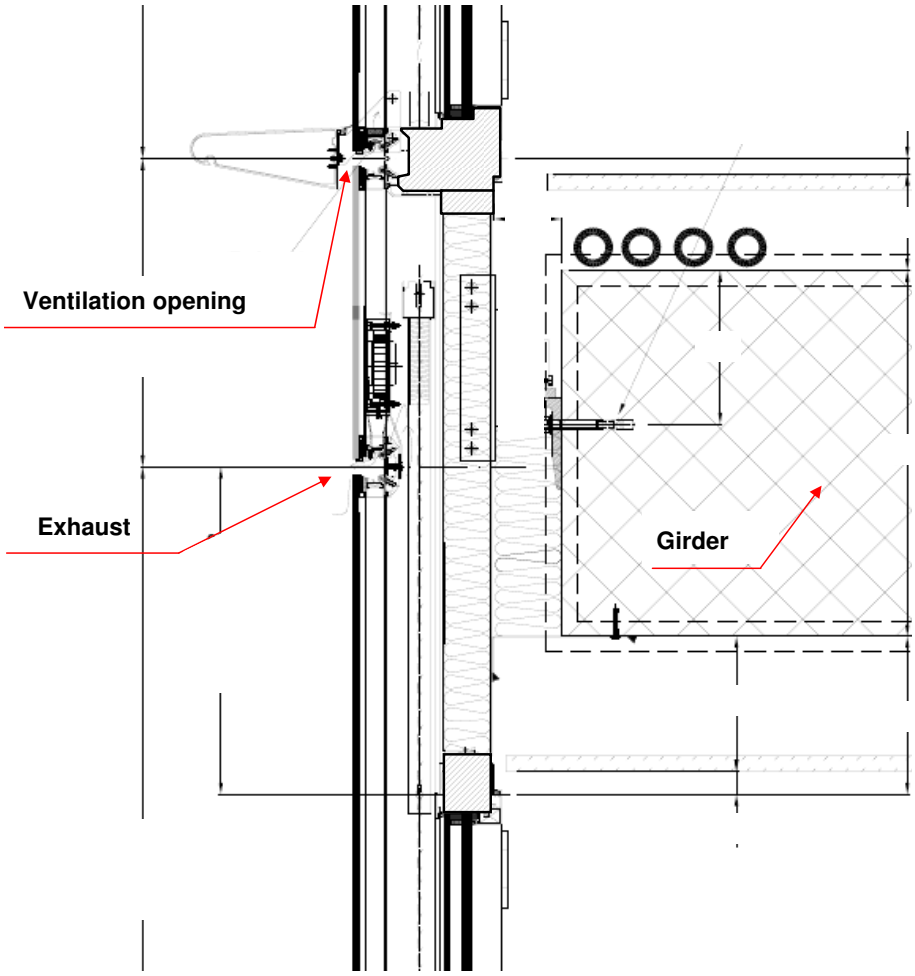

Figure 6.3: *Permasteelisa DSF Section*

The facade section considered is 3455 *mm* high and 1350 *mm* width and is essentially composed by three glazing layers and a Venetian blinder shading device. A scheme of the glazing system is shown in Figure 6.4 and the properties of the glass are reported in Table 6.1 A float glass has been used for all the layers, and the internal side glass was also equipped with a 0.38 *mm* Poly-Vinyl-Butyral sheet.

The venetian blinder is made by 0.2 mm curved aluminum sheet, painted with different colors to test the effects of the paintings on the optical characteristics of the DSF.

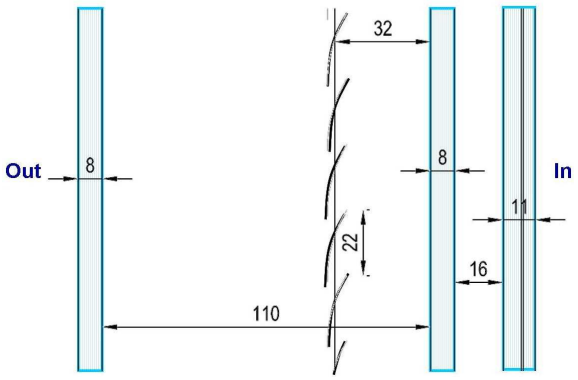

Figure 6.4: *Permasteelisa DSF configuration*

Table 6.1: *Material properties*

	Glass	Blinder
Density $[kg\,m^{-3}]$	2500	2800
Thermal Conductivity $[Wm^{-2}]$	1	160
C_p $[J\,kg^{-1}K^{-1}]$	750	880
Emissivity	0.84	0.84

Cavity ventilation is guaranteed by three centrifugal fans located in the upper part of the section (Figure 6.3) and working in suction mode. Fan characteristic is reported in Figure 6.6 and their positioning is visible in Figure 6.5. During the experiments only two fans were working, ensuring a total flow rate of 40 m^3/h for unit width of facade. The air enters the cavity through openings located in the bottom crosswise frame, as shown in Figure 6.7 and in Figure 6.8.

6.3 Measurement Instruments

Instrument information were provided by Permasteelisa S.p.A. in [43]. A pyranometer has been used to collect information about the total solar radiation. P1–Rh thermocouples have been used to measure the temperatures of the glazings, the Venetian blinder slats and the cavity flow horizontal sections

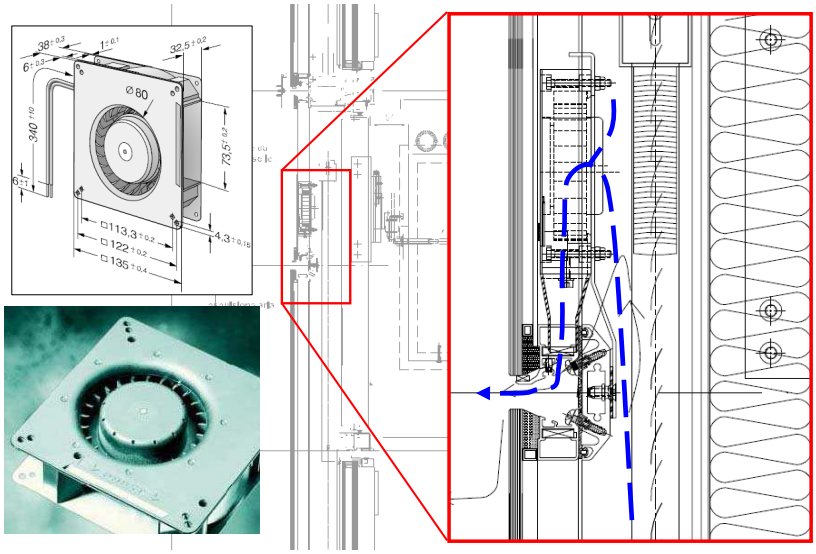

Figure 6.5: *Permasteelisa DSF fans particular*

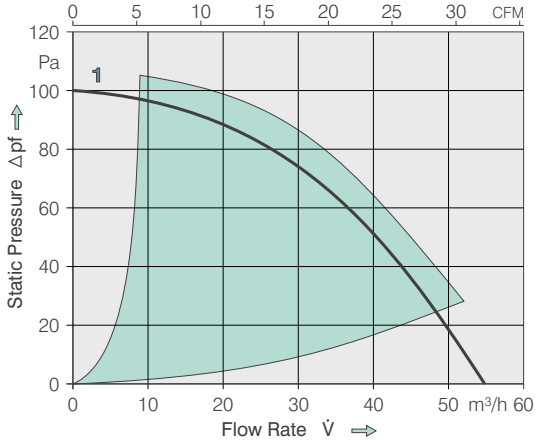

Figure 6.6: *Fan characteristic*

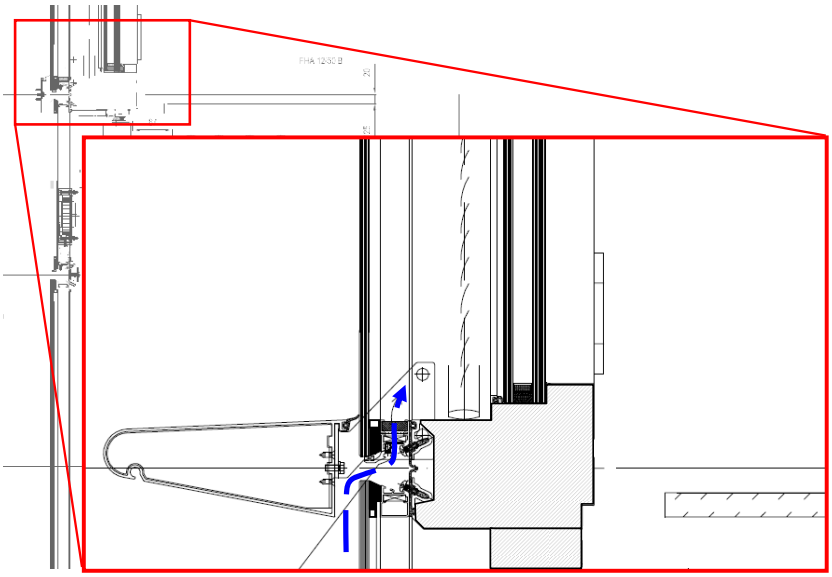

Figure 6.7: *Permasteelisa DSF inlet particular*

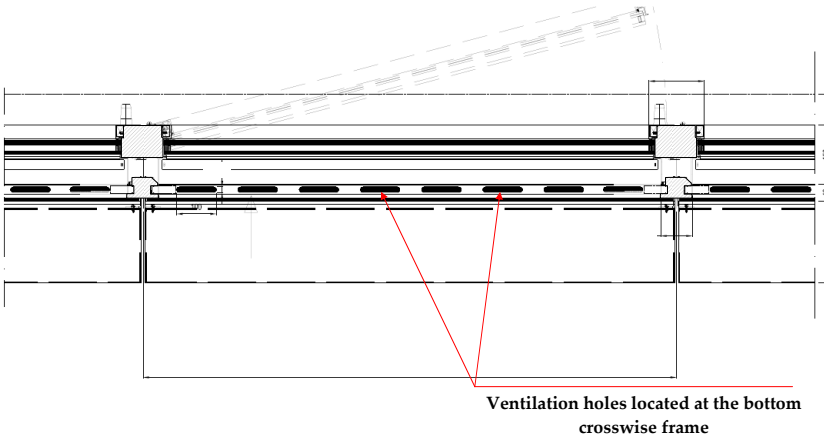

Figure 6.8: *Permasteelisa DSF transverse frame particular*

placed at three different heights: 0.3 m, 0.9 m and 2.0 m from the bottom of the facade. The pictures of the measurement instruments are reproduced in Figure 6.9 and Figure 6.10, while information about the instrument accuracy are summarized in table 6.2.

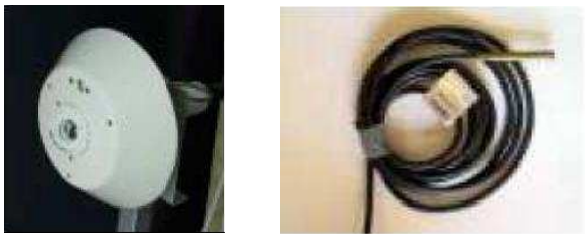

Figure 6.9: *Measurement instruments: Pyranometer (left) and Thermocouple (right) [43]*

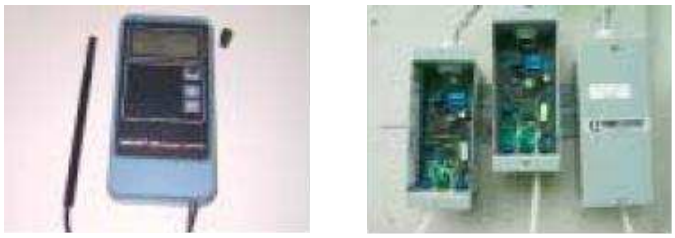

Figure 6.10: *Measurement instruments: Flowmeter (left) and Manometer (right) [43]*

The report provide also some further information about the accuracy of the instruments that are shown in Table 6.2.

Table 6.2: *Measurement instrument accuracy*

Instrument Type	Accuracy [%]
Manometer	$\pm 1\%$
Temperature Sensor	$NotAvailable$
Air Flow Meter	$\pm 5\%$
Thermo Hygrometer	$\pm 0.1C \pm 0.1\%RH$
Pyranometer	1.5%

6.3.1 Measured Data

Data have been collected in different environmental conditions, in different days and time. Four cases have been presented in [43].

Table 6.3: *Studied cases environmental conditions - I: External Irradiation, T_{ext}: External Temperature, T_{int}: Internal Temperature, T_o: Inlet Temperature*

Case	I $[W/m^2]$	T_{ext} $[^oC]$	T_{int} $[^oC]$	T_o $[^oC]$
Case 1	600	27.8	24.4	33.2
Case 2	556	29.6	25.0	37.3
Case 3	691	32.4	26.0	37.6
Case 4	720	32.4	26.5	39.9

For every case are reported the external solar irradiation, external environment and room temperatures and the temperature measured in correspondence of the inlet section. As previously explained, several parameters have been stored:

- Glazing temperature
- Cavity temperature
- Incident solar radiation
- Airflow rate, inlet and outlet flow temperature.

Table 6.4: *Case 1 and Case 2 - Experimental data - Temperature* $[^oC]$

	Case 1			Case 2		
	y = 0.3	y = 0.9	y = 2.0	y = 0.3	y = 0.9	y = 2.0
Glass 1	45.5	53.9	57.2	43.9	48.8	50.1
Cavity 1	41.5	55.7	61.2	40.9	48.7	52.4
Venetian	51.3	62.2	68.6	46.5	54.6	57.6
Cavity 2	44.5	52.4	62.0	41.5	45.4	51.2
Glass 2	43.6	51.6	58.8	39.2	42.9	47.2
Glass 3	28.2	29.8	31.6	27.9	28.9	29.8

Moreover, a meteorological station recorded outdoor climatic data. A supervising and controlling system registered the data from the measurement instruments and managed the air-conditioning system to keep the same internal set-point environment for all the test rooms. The monitoring of the air and

water flow rates and temperatures of the HAVC system, both for heating and cooling, enabled a precise real time evaluation of the energy consumption of the system [44].

Four cases have been presented in [43]. For each case the external solar irradiation, the external environment, the room temperatures and the temperature measured in correspondence of the ventilation inlet section are reported. Data are summarized in Table 6.3.

As previously mentioned flow, glass layers and Venetian blinder slats have been monitored and the measured temperatures are reported in Table 6.4 and in Table 6.5. For the four cases are reported the temperature on three different height. Also the cavity has been monitored and two temperature are reported.

The ventilated cavity may be considered as composed by an external cavity (Cavity 1, between the external glazing and the venetian slats) and an internal cavity (Cavity 2, between the Venetian blinder and the intermediate glazing). The flow in the internal and external cavities has been also monitored and the two temperature are reported.

Table 6.5: *Case 3 and Case 4 - Experimental data - Temperature* $[^oC]$

	Case 3			Case 4		
	y = 0.3	y = 0.9	y = 2.0	y = 0.3	y = 0.9	y = 2.0
Glass 1	50.4	57.6	61.1	51.5	59.5	63.2
Cavity 1	46.7	59.2	64.9	48.1	61.8	68.2
Venetian	55.6	65.9	71.3	59.8	70.0	76.5
Cavity 2	48.9	54.9	63.4	51.2	58.2	69.2
Glass 2	46.5	53.7	59.9	48.5	56.6	64.5
Glass 3	29.7	31.2	32.3	30.9	32.4	34.0

Chapter 7

Double Skin Facade CFD Simulations

7.1 Introduction

In the previous chapters a preparatory study for the investigation of a full Double Skin Facade has been provided. A step–by–step validation of the CFD procedures to perform suitable simulations of the typical indoor ventilation phenomena has been also reported.

In this chapter a comprehensive investigation of a full DSF system will be provided together with a critical analysis of the results and of the comparisons with the experimental data illustrated in sec. 6.

As described in sec. 3.3 and in sec. 4.3 the radiation heat transfer introduces an additional challenge in order to reproduce the physical phenomenon through a CFD simulation. The radiation models embedded in the CFD code proposed to perform the simulations, and in particular the DO radiation model, seem not to be a completely validated feature according to the recent literature. In this chapter, a *decoupling method*, will be used to take into account the radiation heat transfer (see sec. 7.3 for details).

WIS software [45] (see sec. 7.2) has been used to calculate facade layers optical properties. Then the net energy balance of the facade has been calculated taking into account every layer and the resulting values have been inserted in the CFD code to independently solve the thermal analysis. A brief description of the WIS software and its main features is provided in the next section.

The investigation will also include three–dimensional and two–dimensional modeling to determine if the thermal and fluid flows may be considered two–dimensional under some assumptions. Grid refinement analysis has been also performed to guarantee the grid independence of the results.

Finally a comparison of the results with the experimental data will be shown.

7.2 The WIS software

WinDat project (Windows as Renewable Energy Sources for Europe Window Energy Data Network) started as a European Thematic Network, financially supported by the European Commission (2001-2004). WinDat aims to make available and freely distribute a European software tool (WIS) for the calculation of the thermal and solar properties of commercial and innovative window systems on the basis of known component properties and thermal and solar/optical interactions between the components [46]. The original WIS tool has been developed in the *Advanced Windows Information System (WIS)* project (2004-2006) financed by the Directorate General XII for Science, Research and Development (2004-2006), co-ordinated by TNO Building and Construction Research.

7.2.1 European Standard Normative

European Commission is directly involved through the *European Committee for Standardization* (CEN) in the development of standards that could be the guideline for windows and advanced glazing systems producer and designer. Several CEN publications about glazing production, measurement and properties definition have been published or renewed in last years.

The main reference European Standards for glazing design and production are:

- prEN 13119:2004 *Curtain walling – Terminology*
- EN 410:2000 *Glass in buildings – Determination of luminous and solar characteristics of glazing*
- EN 673:2005 *Glass in buildings – Determination of thermal transmittance (U-value) – Calculation method*
- EN 13363-1:2006 *Solar protection devices combined with glazing – Calculation of solar and light transmittance – Part 1: Simplified method*
- EN 13363-2:2006 *Solar protection devices combined with glazing – Calculation of total solar energy transmittance and light transmittance – Part 2: Detailed calculation method*

7.2.2 WIS Software Description

WIS is a multi–purpose, PC based European software tool to assist in determining the thermal and solar characteristics of window systems (glazing, frames, solar shading devices, etc.) and window components. The tool contains databases with component properties and routines for calculation of the thermal/optical interactions of components in a window [45].

The first simplifying assumption in the WIS model, as explained in [45], is that the thermal and solar properties of a transparent system may be considered

as one-dimensional, perpendicular to the pane surface. Two-dimensional effects are taken into account where this is an obvious oversimplification, for example in thermal driven ventilation.

Two calculation modes are available in WIS. In *CEN only mode* all calculations are performed according to the European standards provided by the European Committee for Standardizations (CEN). Following the prescriptions of the standard EN 410 and EN 673, WIS calculates solar factor, light and UV transmittance and general color rendering index of single glazings and multi-glazing systems without solar shadings, U-value and surface temperatures of the center parts of each pane (see [45] for details).

In *expert mode* all calculations are performed according to the physical principles which are the basis for the European standards used in CEN only mode. Moreover, in this mode the U-value of multi-glazing systems with films or other layers which are permeable for thermal radiation can be calculated together the U-value of a window with shutters or blinds and the effect of thermally driven air circulation and forced air circulation with known air exchange rate. Furthermore there are some optional calculations such as fitting optical properties for angles.

7.2.3 WIS Software Results

For the purpose of this work WIS results have been provided by Permasteelisa R&E Department about the optical properties of the DSF described in chapter 6.

The analysis of these data have been performed in order to define the actual optical parameters of the glazing system during experimental campaign. In Table 7.1 are described the parameters that characterized the studied DSF and that will be used in the next sections.

Table 7.1: *WIS calculated Global Facade Properties - ρ: Reflactance, α_i: Absorbance, τ: Transmittance*

Coefficient	Case 1	Case 2	Case 3	Case 4
ρ	0.2450	0.2910	0.2450	0.2330
α_1	0.2340	0.2420	0.2340	0.2280
α_{VB}	0.4830	0.4370	0.4830	0.5010
α_2	0.0124	0.0099	0.0124	0.0128
α_3	0.0086	0.0068	0.0086	0.0089
τ	0.0162	0.0068	0.0162	0.0167

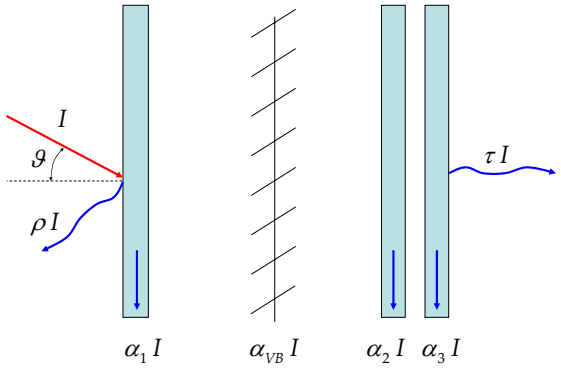

Figure 7.1: *Scheme of the final optical properties from WIS software*

7.3 Decoupling Method

Regular window systems can be essentially examined as a one–dimensional system. The thermal resistances can be considered parallel connected and a system of equation can be relatively easily created [14].

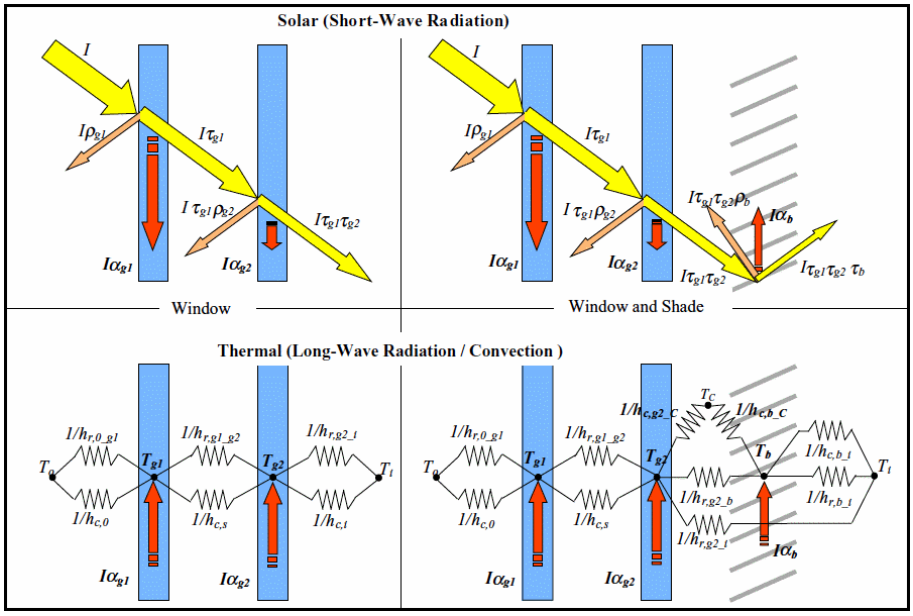

Figure 7.2: *Solar and thermal energy transfer in a shaded an unshaded window. Inter-reflections have been omitted for clarity [14]*

With the addiction of a shading layer such as a Venetian blinder the analysis

of thermal resistance network becomes more complex and consequently the whole system is more difficult to analyze.

In [47] in order to determine the solar heat gain coefficient (SHGC) of a multi–layer shaded glazing system a method was developed using two strategies named by the authors as *solar–thermal separation* and *layer method*. Thermal–solar separation introduces the assumption that short wave solar radiation can be examined separately from long wave heat transfer.

In the layer method the fenestration is broken up into a series of plane–parallel layers and the system optical properties are calculated from the bidirectional optical properties of the the individual layers through a scanning radiometer. Therefore through an optical analysis of the system it is possible to determine directly transmitted, reflected and absorbed components of solar irradiation. Finally the absorbed component can be used as input into a thermal analysis that is solved independently [14].

Figure 7.2 demonstrates the cited analysis for a shaded and an unshaded glazing system positioned, in this case, in the internal side of a double-glass window. It should be noticed that the classical similarity between thermal exchanges and electric circuits, as explained in [28], has been embedded in the procedure.

The same approach could be applied to a shaded DSF. Optical properties of the layers should be calculated following a scheme similar to the *short wave radiation* scheme in Figure 7.2. Then the thermal exchanges in a classical DSF commercial configuration can be solved following the *long wave radiation–convection* that may be represented as in Figure 7.3. Inter–reflections have been omitted for clarity of representation. Convective (h_c) and radiative (h_r) thermal resistances between the different layers are shown from outside to inside. The orange arrows represent the absorbed energy calculated starting from the optical properties of the facade layers.

The decoupling method proposed for DSF investigation separates the optical and thermal analysis, uses WIS software for optical facade layers calculations and performs a CFD thermo–fluid dynamic analysis based on WIS results.

The results of WIS software calculations for the Permasteelisa facade (see Chapter 6, also reproduced in Figure 7.1) are shown in Table 7.1. The solar irradiation angle of incidence has been calculated for every case, according to the test room geographic position, the date and the time of the measurements. Thus optical properties related to the specific incidence have been extracted from WIS results.

The net transmitted (τI), absorbed (αI) and reflected (ρI) part of the incident radiation (I) by the facade layers is specified following the scheme shown in Figure 7.1. It is well known that part of the energy absorbed by a body will be re-emitted at the equilibrium according to the Stefan-Boltzmann Law and depending on the emissivity of the surface. The process scheme for the facade layers is shown in Figure 7.4.

The radiation energy balance of the whole facade has been calculated and

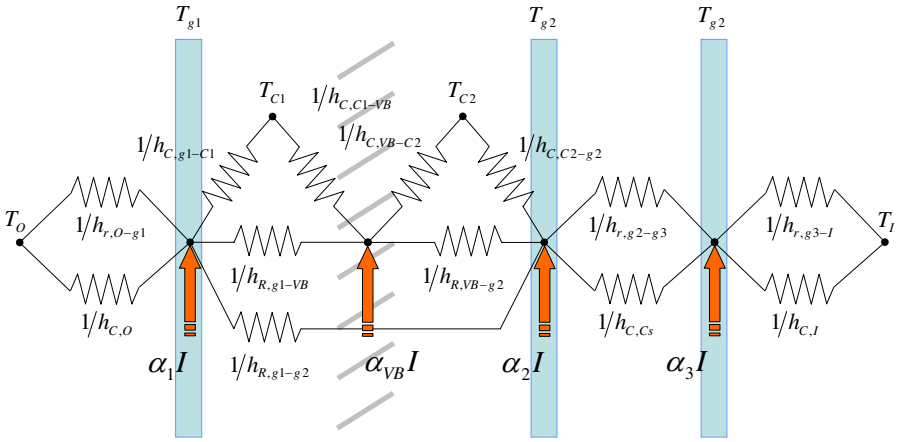

Figure 7.3: *Solar and thermal energy transfer in a shaded DSF. Inter-reflections have been omitted for clarity*

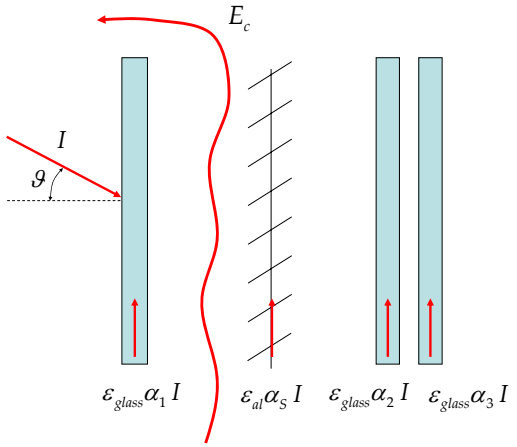

Figure 7.4: *Scheme for thermal calculation*

the re-emitted energy part of every skin has been set as a heat generation rate in the boundary condition for a CFD software (see sec. 7.4.2 for details about boundary conditions).

7.4 Double Skin Facade Simulations

7.4.1 Computational Domain and Grid

The simulation of a complex three–dimensional geometry requires generally high costs in terms of computational time. Thus assumptions and simplifications are commonly adopted when a large number of different simulations are required. Of course this approach requires a continuous analysis of the results to avoid that adopted criteria could affect the simulation in a undesired way.

Since this work is preparatory to a parametric investigation on DSF, improvement of computational time becomes a relevant criteria for the modeling choices. The first step in this direction has been to perform a grid independence analysis and then to evaluate if the thermal and fluid flows in the facade could be considered two–dimensional.

A three–dimensional model has been built with spatial discretizations following the advices proposed in [8]. Details about boundary conditions and grid grading near to the solid boundary will be discussed later.

The geometry has been simplified by not modeling the exhaust fans and omitting the bearing parts of the Venetian blinder. Slats have been reproduced as shell surfaces and the curve shape has been simplified with a flat rectangular surface.

A vertical section of the computational domain is shown in Figure 7.5 and three–dimensional views are shown in Figure 7.6. The computational domain is 3.455 m height and 1.35 m depth in three dimensional configuration. Layers thickness and cavity width are shown in the DSF section scheme represented in Figure 6.4 reported also in Figure 7.7 for convenience.

Triangular mesh has been used to discretize the cavity fluid zone. Unstructured grid has been chosen for a planned future development of the work where an arbitrary slat position might be selected and where a rapid grid generation would be appreciated. Cartesian mesh has been used only for solid zones.

Grid independence has been established through results obtained from different size meshes. Two–dimensional simulations have been finally performed with a mesh composed by 3×10^5 cells. The three-dimensional model has been built with a mesh of about 2.5×10^6 cells.

7.4.2 Numerical Model and Boundary Conditions

Two equations eddy viscosity k-ϵ turbulence models are commonly adopted in indoor environment heat transfer situations as described in Section 4.2. Different k-ϵ model formulations have been analyzed by Chen [8] in natural, mixed

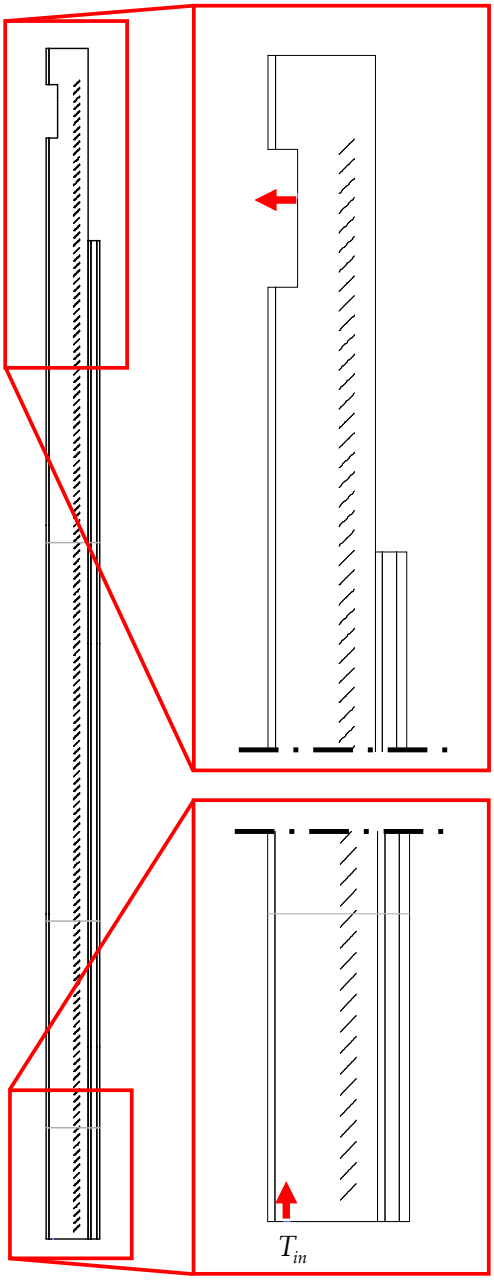

Figure 7.5: *Computational domain*

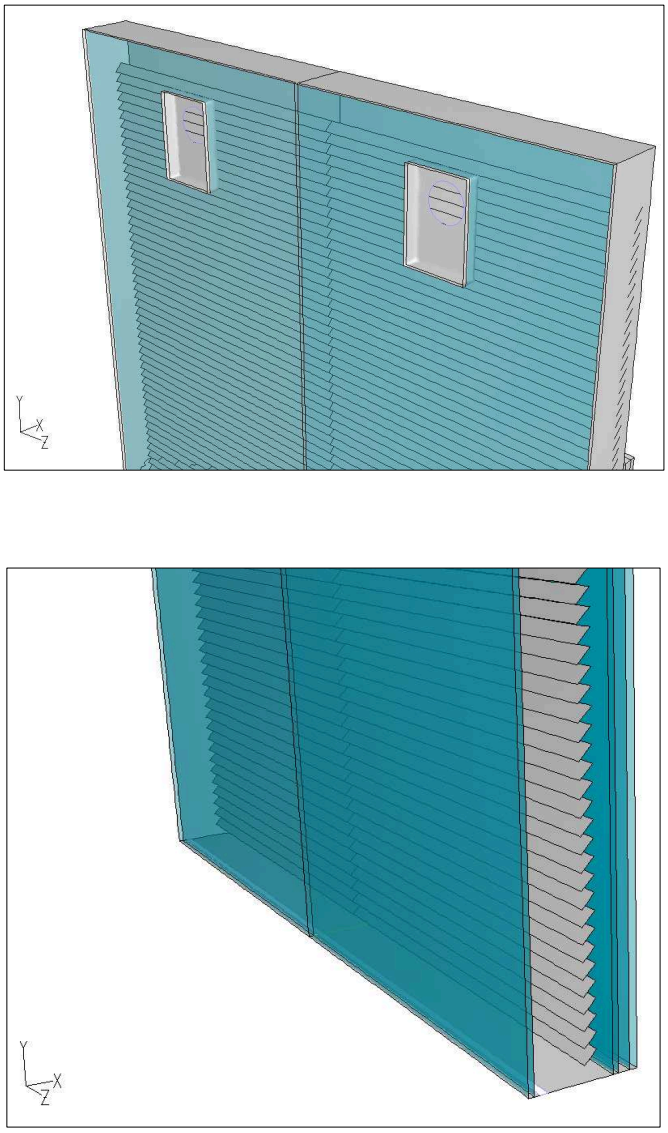

Figure 7.6: *3D simplified model*

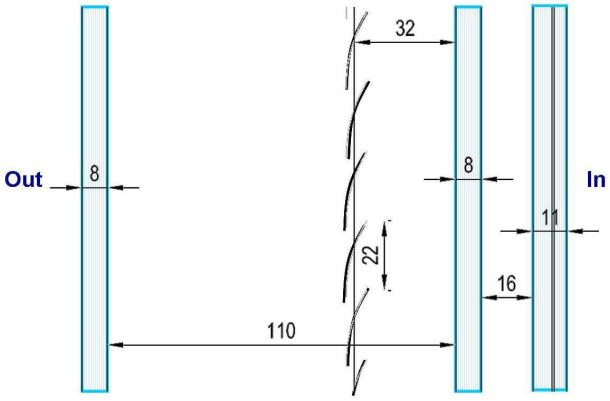

Figure 7.7: *Permasteelisa DSF configuration*

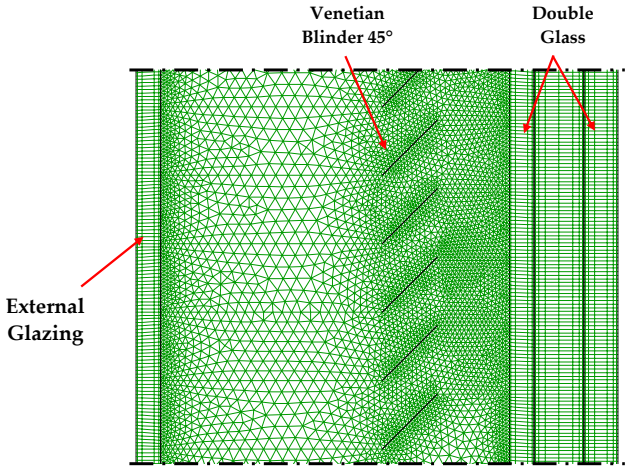

Figure 7.8: *Computational Discretization*

and forced convection standard conditions. RNG variation of the standard k-ϵ model is then recommended for indoor air flow simulations.

Boussinesq approach has been used for density (see sec. 4.2.3). The SIMPLE model has been employed for velocity-pressure coupling and second order discretization has been set. The finite volume commercial software Fluent 6.3© has been used in order to numerically solve the governing equations [35].

The initial distribution of k and ϵ have been assumed to be $10^{-3}m^2/s^2$ and $10^{-5}m^2/s^3$ as suggested in [48].

No-slip boundary condition on the velocity components has been applied for all the walls. During simulations y^+ values have continuously monitored in

order to improve the grid configuration to obtain a suitable value of about 10 as suggested in [8] using *wall functions*.

Air inlet and outlet sections have been simplified by an equivalent rectangular area section. Outlet fan section has been simplified in 2D model and the complete fan sections have been reproduced in 3D model as shown in Figure 7.6.

The experimental flow rate generated by the two working fans has been guaranteed through a fixed outward velocity boundary condition. The use of a *velocity inlet* boundary condition to define flow velocity at flow exit it is allowed in Fluent under the safe condition of monitoring the overall continuity in the domain [35].

The Rayleigh number calculated in respect of the cavity height is 10^{11} as order of magnitude for all the presented cases. Reynolds number is 1×10^4 in respect of the cavity width.

At the inlet an *intake fan* boundary condition has been set with null pressure jump and gauge total pressure. Intake fan boundary condition is similar to the pressure inlet, but in this case the pressure drop inside the domain due to the topside fans determines an inward flow through the inlet section. The turbulence intensity I at the inlet section has been set at 15% [48].

A positive energy source have been set for simulate the re-emitted heat from glazing layers and Venetian blinder slats following the convention that all positive source terms indicate energy introduced in the domain and all negative source terms indicate energy extracted from the domain. In equation 4.4 the defined energy source will appear in the S_h term.

7.5 Results

It is well known that in these problems to obtain a good numerical convergence it is challenging, due to the high aspect ratio and the high Rayleigh number present in convection–led flows. In [35] some procedures are suggested to improve convergence in these cases.

A typical trend of the convergence history related to a two–dimensional simulation is shown in Figure 7.9. Residuals are defined for a segregated solver as explained in [35]. First order discretization shows a good convergence after 1000 iterations. The sudden jump in the graph indicates that the discretization has been set to the second order and it appears clear how the solver presents some difficult to achieve the same residuals values reached with the first order. This evidences once more how challenge is to perform high quality simulations in domains where complex phenomena occurs.

However residuals related to the energy equation shows a good trend also with a second order discretization. The variables related to the energy equation and mainly the temperature are of great importance for the global result of the simulation.

As mentioned it is important, in order to reduce the computational cost, to

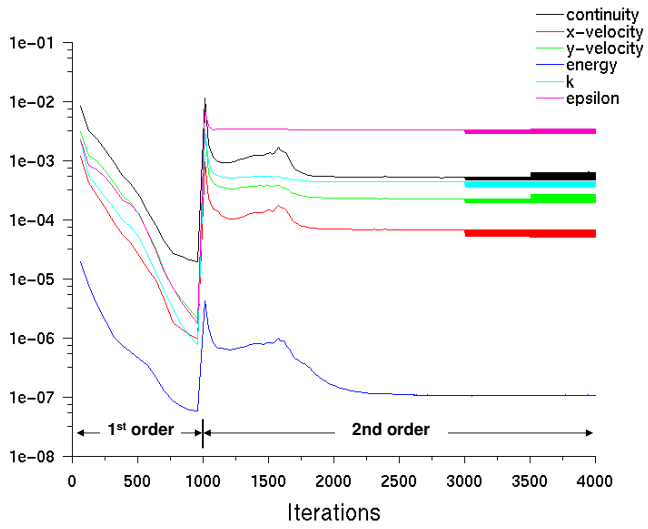

Figure 7.9: *Convergence history – Trend of residual Case4*

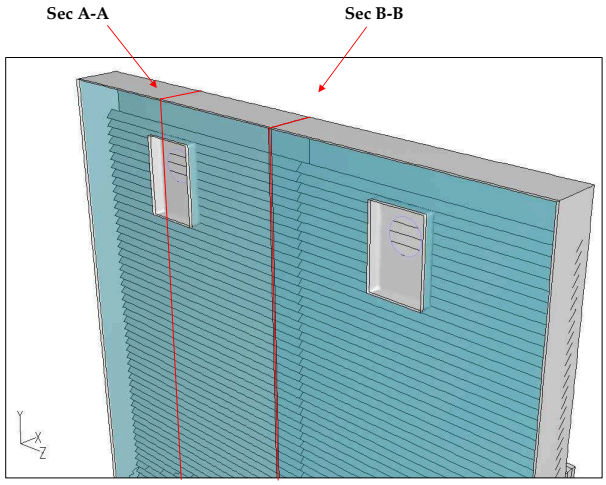

Figure 7.10: *Reference measurement planes for 3D contour plot*

evaluate if both the thermal and fluid flows in the facade could be considered two–dimensional. Firstly, two-dimensional and three-dimensional comparisons of isothermal maps for Case1 are shown in Figure 7.11. Perpendicular slices to the glazing planes have been cut for contour plot.

Temperature plots in the top and bottom sides of the facade are represented in Figure 7.11. On the left the 2D results are shown and on the right the 3D results referred to section A–A and section B–B are reported, following Figure 7.10 scheme. It is noticeable that the facade part upside the exhaust fan reaches a higher temperature in the 3D model, probably depending on the flow concentration toward the suction mouth of the fan. The temperature contour plot comparison for the inlet side of the DSF exhibits a good agreement between the 2D and the 3D models results. For a two–dimensional Case1, the flow field prediction is represented in Figure 7.12 through a velocity vectors plot showing that above the exhaust fan a vortical structure occurs. In the bottom side of the window the inlet air flow incoming close to the external glazing layer separates in two directions after moving through the Venetian blinder toward the internal cavity. One part moves upward and another part moves downward creating recirculating zone.

An overview of the path lines is visible in Figure 7.13 for three–dimensional case. Again the separation of the flow, as discussed above, is confirmed together with the complex flow in the upper side of the window.

Horizontal slices have been defined in the computational domain in order to plot temperature contours at different height. In Figure 7.14 eight planes $50\,cm$ spaced are presented. The temperature field appears mainly bi-dimensional. Some differences can be noticed near the inlet section where the flow probably presents a local vortical phenomenon, and in the top side where the exhaust fans generate an obvious three-dimensional flow.

In Figure 7.15 non–dimensional z–velocity contours are shown in the horizontal slices. Z–velocity component has been non–dimensionalized by the velocity magnitude at the same point. Figure 7.16 confirms that three–dimensional vortices develop stronger as the height in the facade increases, changing their structure and position in the horizontal planes.

Table 7.2: *Studied cases environmental conditions - I: External Irradiation, T_{ext}: External Temperature, T_{int}: Internal Temperature, T_o: Inlet Temperature*

Case	$I\ [W/m^2]$	$T_{ext}\ [^oC]$	$T_{int}\ [^oC]$	$T_o\ [^oC]$
Case 1	600	27.8	24.4	33.2
Case 2	556	29.6	25.0	37.3
Case 3	691	32.4	26.0	37.6
Case 4	720	32.4	26.5	39.9

Since the experimental data have been collected in the four different environ-

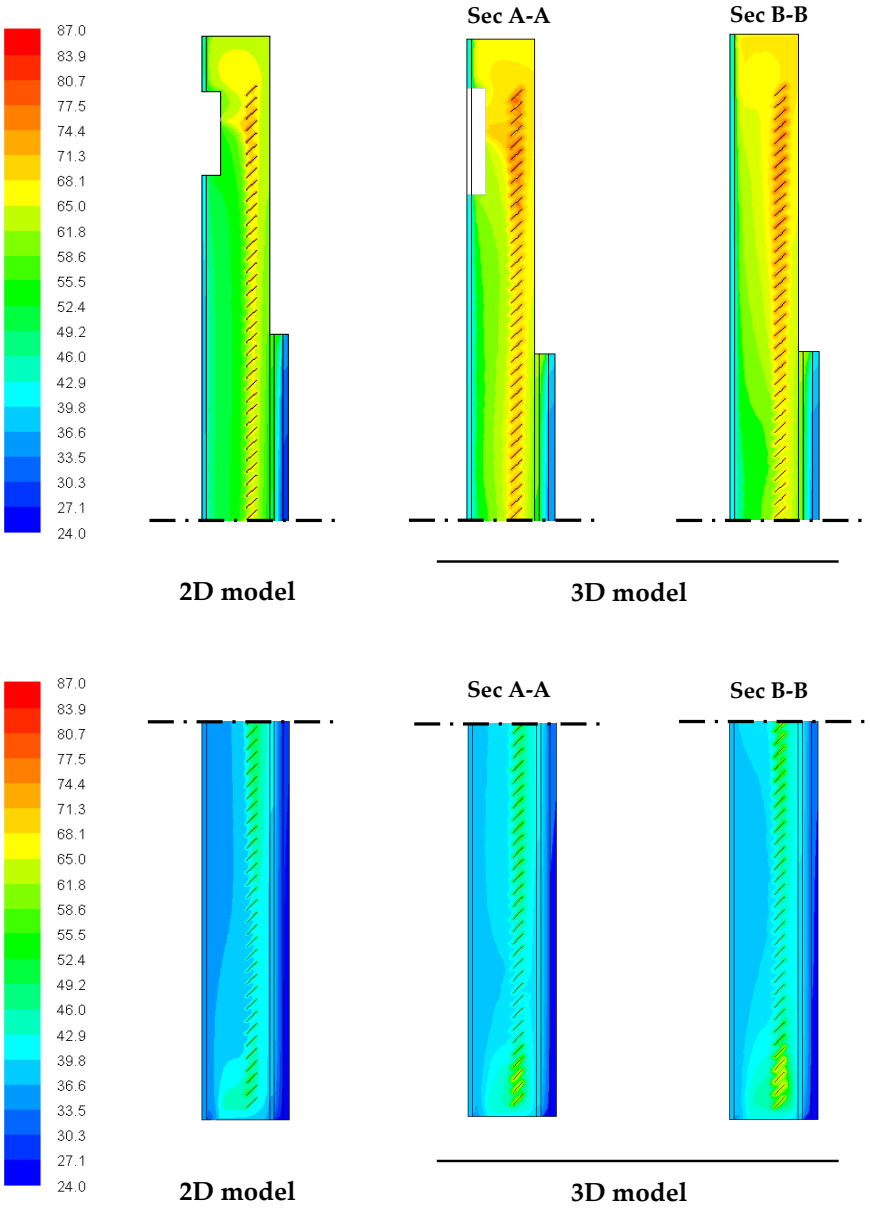

Figure 7.11: *Temperature contour plot comparison between 2D and 3D models in the DSF Top and Bottom sides*

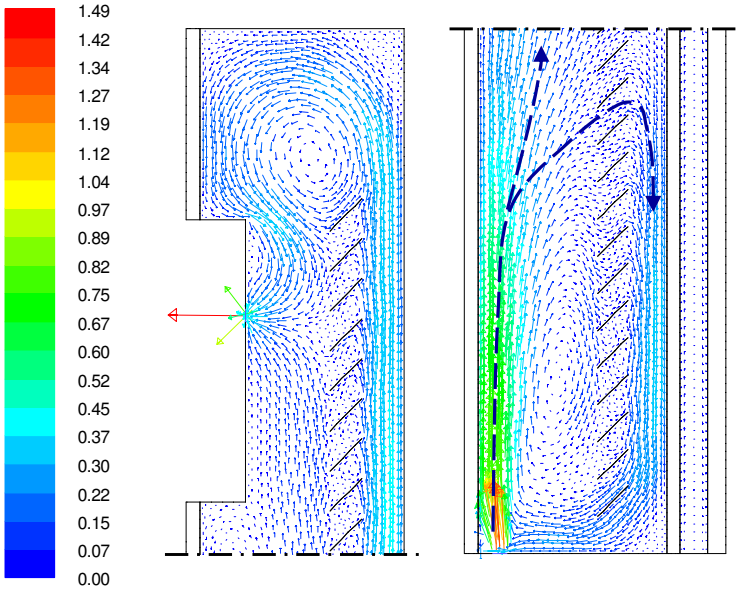

Figure 7.12: *Predicted flow field with velocity vectors in Case1 – 2D case*

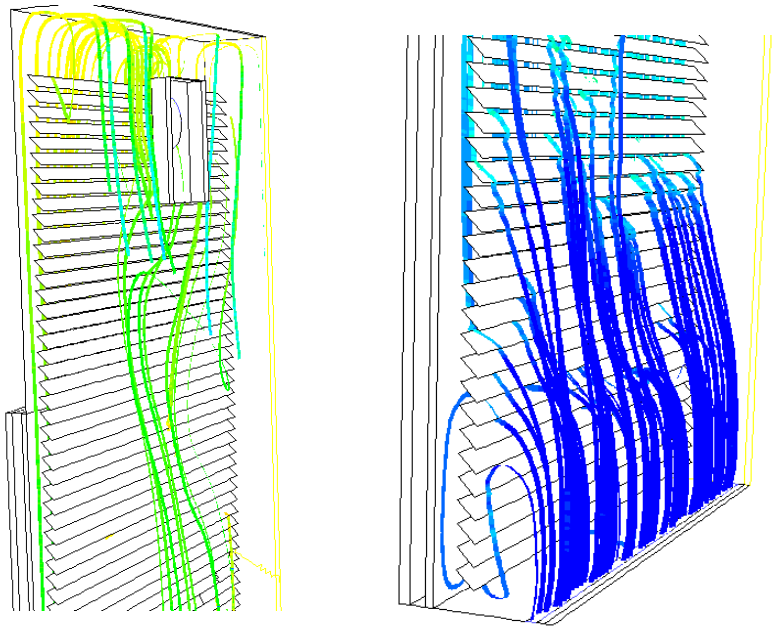

Figure 7.13: *Predicted path lines in Case1 – 3D case*

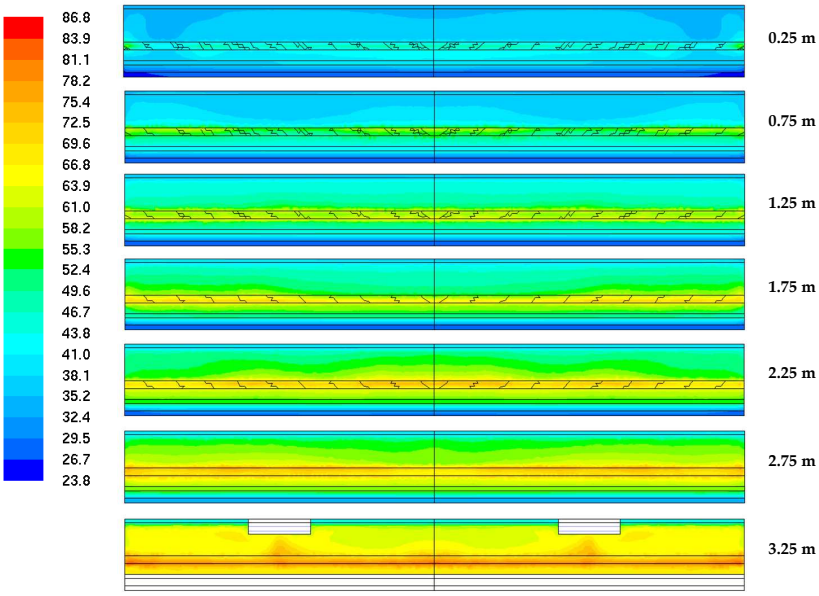

Figure 7.14: *Temperature contour plot on horizontal planes – Case1*

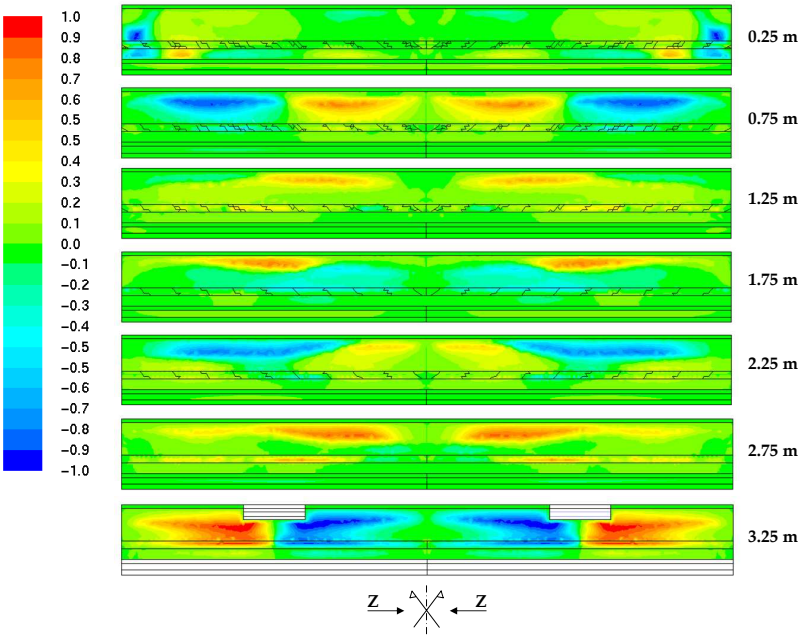

Figure 7.15: *Non–dimensional z–velocity contour plots on horizontal planes – Case1*

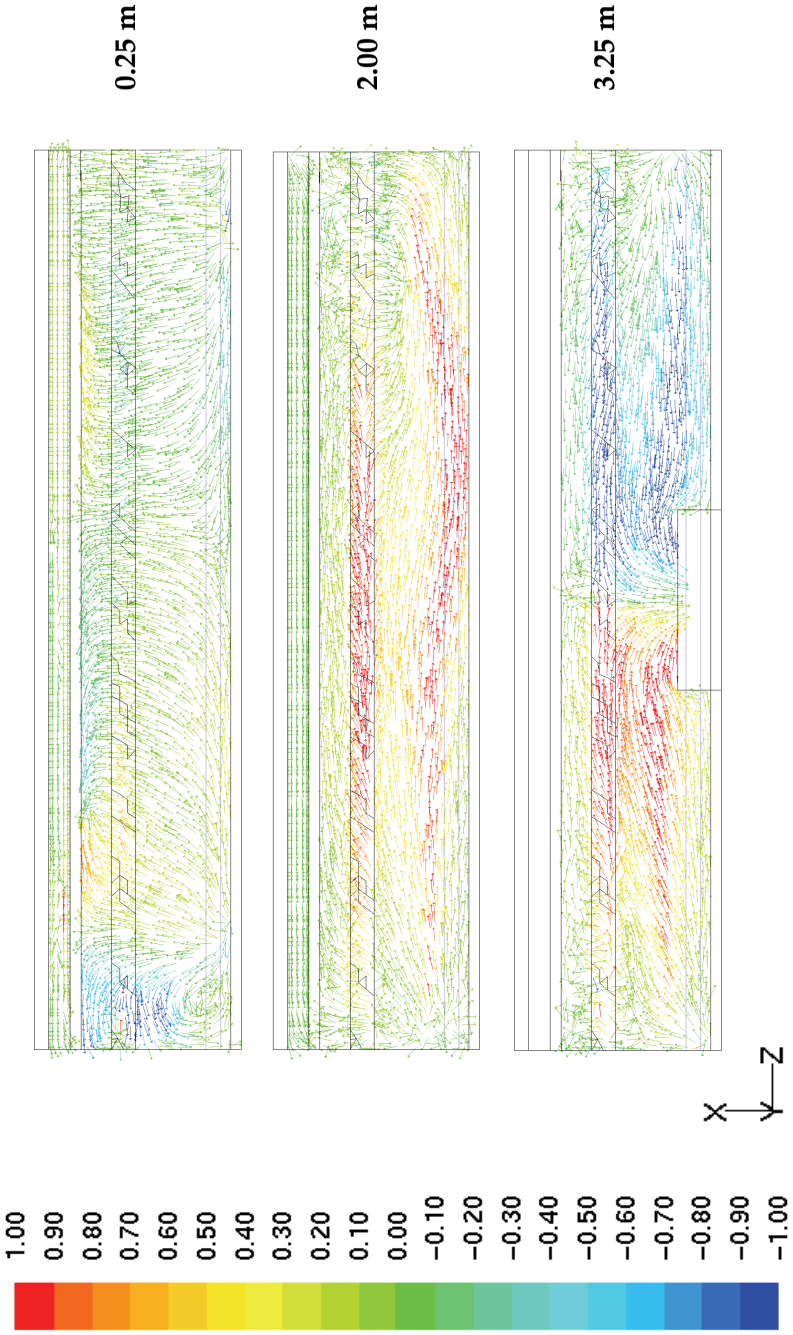

Figure 7.16: *Velocity vectors colored with non-dimensional z-velocity on horizontal planes – Case1*

mental condition, reported again in table 7.2 for convenience, four simulations have been carried out and temperature comparison is reported in Figure 7.17 for Case1 and Case2 and for 2D and 3D models.

In the vertical plane, three horizontal lines corresponding to three different height (0.3 m, 0.9 m and 2.0 m) have been considered to extract predicted results, corresponding to the measurement sections considered in Permateelisa experimental data. Regarding the three–dimensional case the lines belong to the vertical symmetry plane (section B–B if referred to Figure 7.10). The vertical cyan lines represent the tracks of the three glazing layers and the dotted red line indicate the slats axis. The black lines represent the 2D predictions and the red lines represent the results for the 3D model. From left to right the three graphs respectively represents the three different height. Case3 and Case4 results are shown in Figure 7.18.

The results show a general agreement between the 2D and 3D predictions. A slight misalignment is noticeable at $Y = 0.9$ m for every simulated case, and it is particularly evident in Case4. A possible explanation of this trend is the strong 3D flow the develops at about 1 m from the bottom of the DSF as previously discussed.

The temperatures for every glass layer are in close agreement in all the considered cases. Just at $Y = 2.0$ m, Case1 and Case3, a discrepancy is present for the second glazing. An explanation of this phenomenon is not so evident. Analyzing the Figure 7.15, it is shown that z–velocity near the symmetry section changes its sign at about $Y = 2.0$ m, highlighting a three–dimensional flow pattern that may significantly influence the the thermal boundary layer on the glass surface.

Despite the complexity of the flow field, and because the temperature is mainly involved in the purpose of this work, in the following it seems to be possible and convenient to assume that the thermal DSF field is two–dimensional.

The final validation of the procedure for the thermal field evaluation should be conducted by comparison with experimental results.

So far a step–by–step validation has been conducted using both experimental and numerical data found in literature, and the comparison allows to be confident with the accuracy of the simulations. However, since experimental data are available, an evaluation will be performed in the following, taking into account that only a qualitative comparison is possible due to the lack of information about measurements accuracy as mentioned in chapter 6.

In Figure 7.19 the experimental data for Case1 and Case2 are compared with the numerical 2D predictions for the sections previously described. It is reminded here that thermocouple data indicate glass layers, Venetian blinder slats and cavity flow temperatures. Figure 7.20 shows the same comparison for Case3 and Case4. Case1 shows significant differences difficult to explain and this will be taken into account in the analysis of the results.

It is noticeable that the temperature trend in the most internal side of DSF fairly agrees with experimental data. Differences are clearly identified in the external cavity and mainly in the external glass temperature, and this

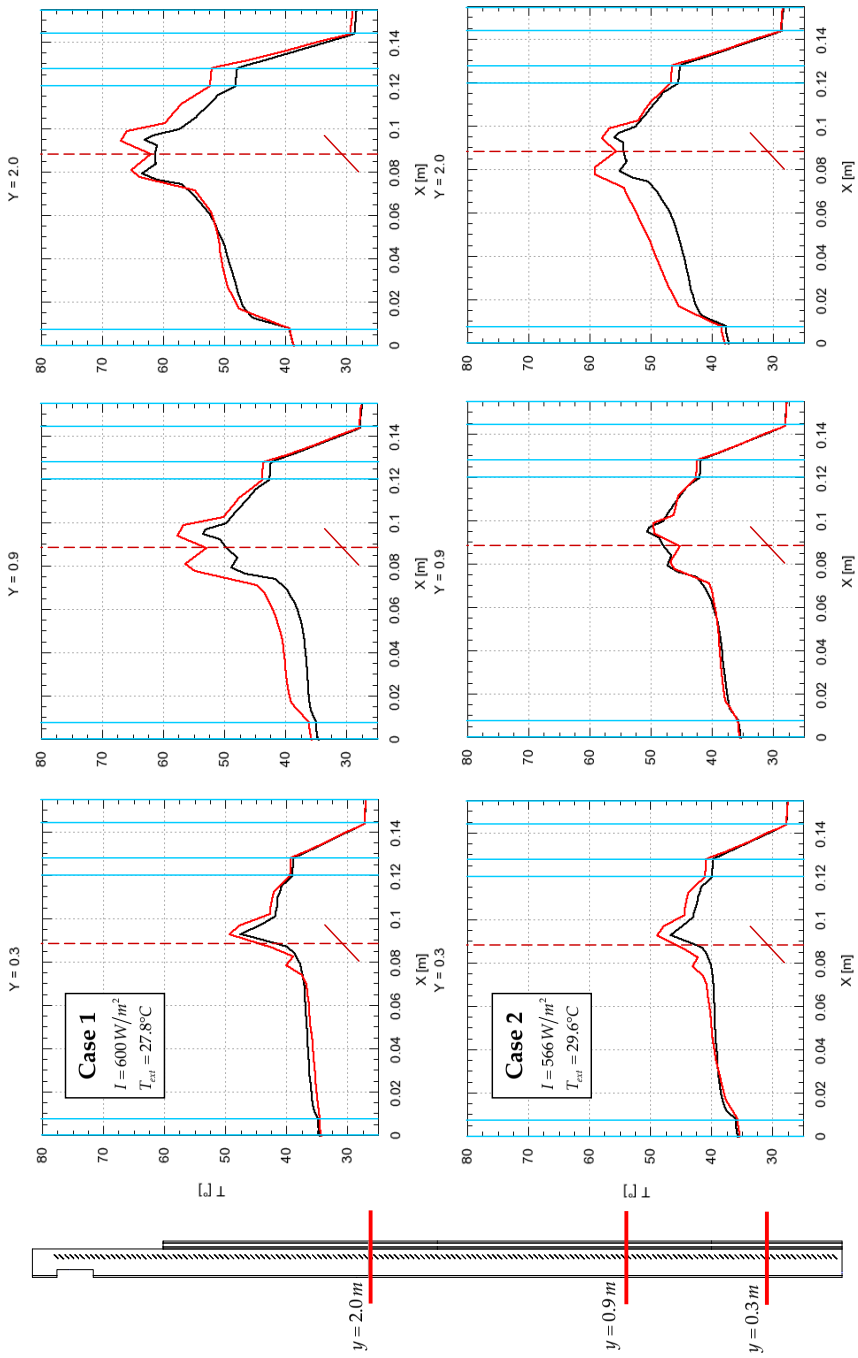

Figure 7.17: *Results comparison between 2D (black line) and 3D (red lines) models: Temperature – Case1 and Case2*

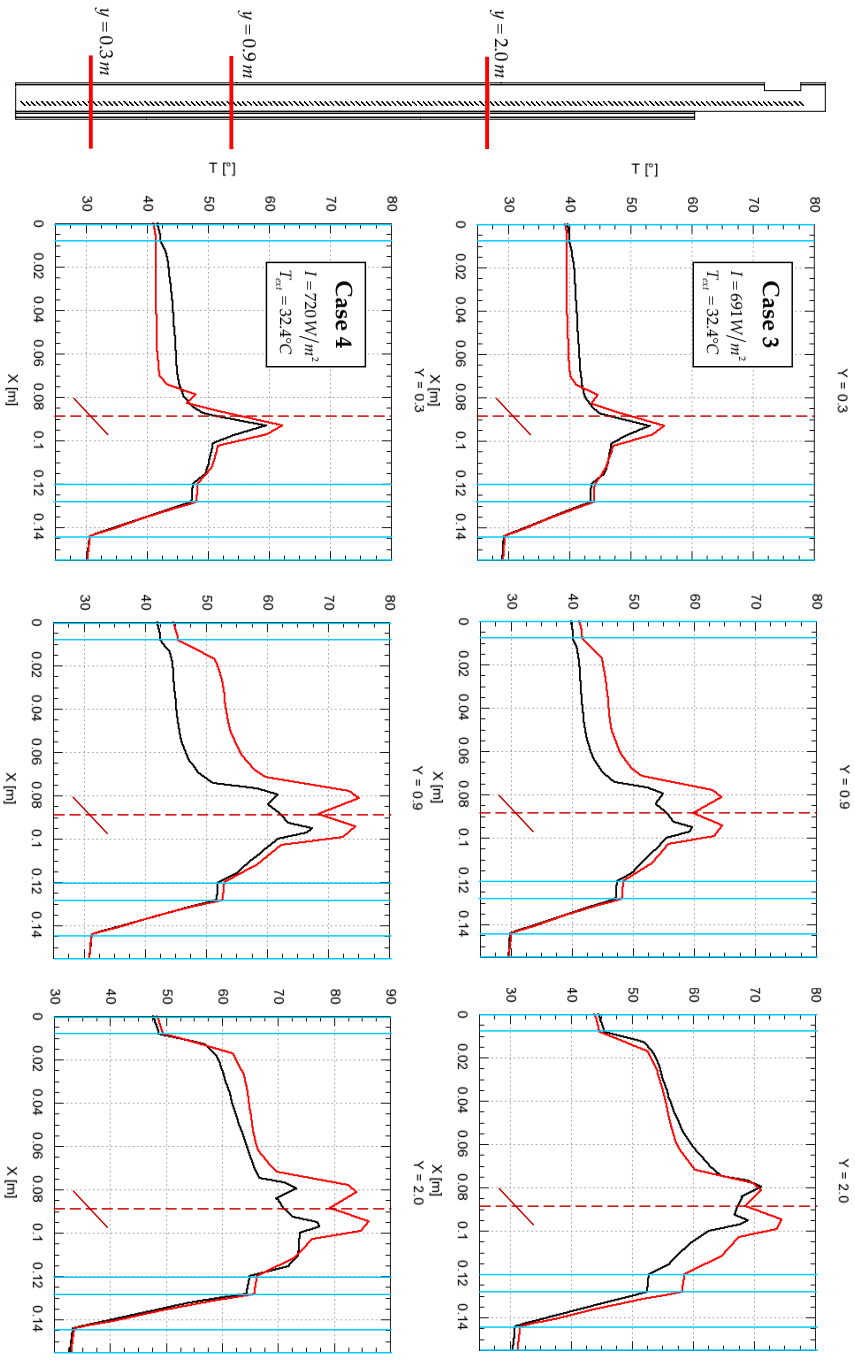

Figure 7.18: *Results comparison between 2D (black line) and 3D (red lines) models: Temperature – Case3 and Case4*

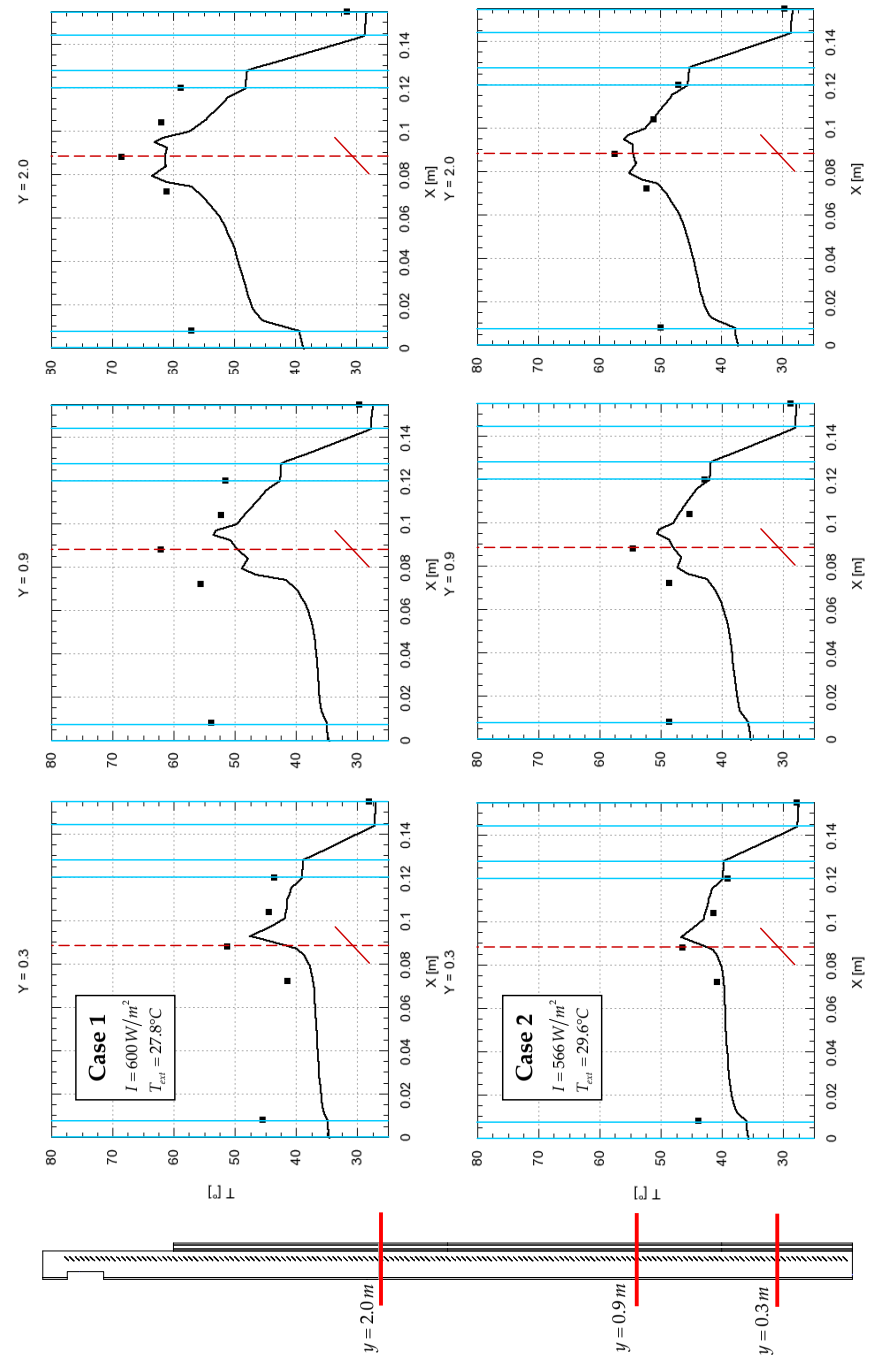

Figure 7.19: *Results comparison: Temperature – Case1 and Case2 – ■: experimental data; —: predicted values. The vertical cyan lines represent the tracks of the glass and the dotted red line the slats axis*

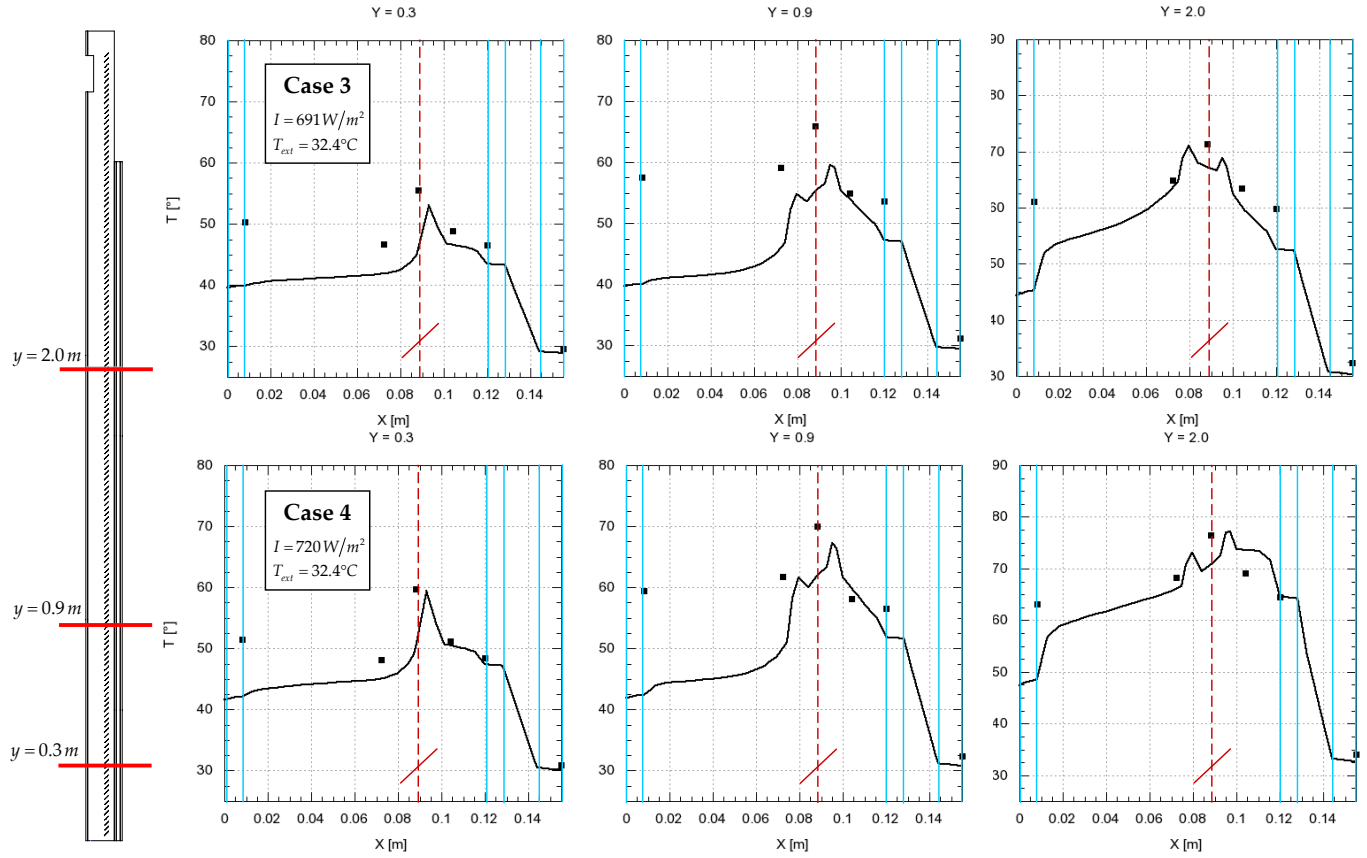

Figure 7.20: *Results comparison: Temperature – Case3 and Case4 – ■: experimental data; —: predicted values. The vertical cyan lines represent the tracks of the glass and the dotted red line the slats axis*

behavior is common for all the studied cases. Only in the section $Y = 0.9\ m$ some differences are evident in the slat temperature, but it has been already mentioned that a strong 3D flow is present in this zone of the DSF. This is confirmed by Figure 7.17 and Figure 7.17 where higher temperature are found for 3D simulations at $Y = 0.9\ m$.

In order to explain this phenomena several simulations have been firstly performed with different values of the external convective heat transfer coefficient h_c, because no information about this parameter were provided. The results in Figure 7.19 and in Figure 7.20 are referred to $h_c = 12\ W/m^2K$. Unfortunately the trend of the predicted results always remains different from the experimental data in the external cavity.

After a review of the experimental campaign reports, it seems possible that a systematic error in the measurements of the external glass temperature is present. Probably the thermocouple has not been properly shielded so that solar direct radiation generated an erroneous evaluation of the temperature.

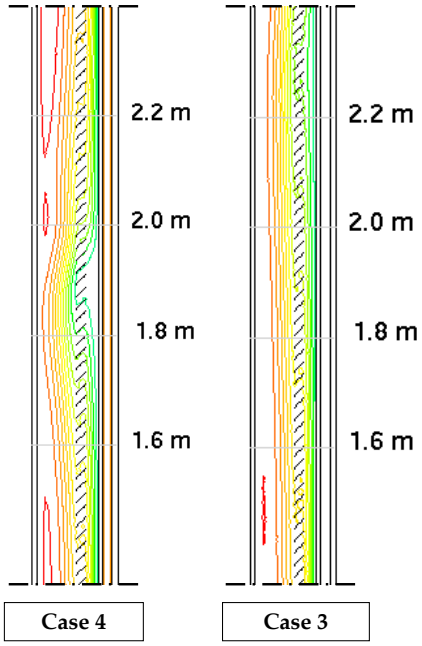

Figure 7.21: *Path lines comparison for Case3 and Case4*

It is interesting to focus to Case3 and Case4 results. As shown in Table 7.2 the measurement have been collected with the same external and internal temperature, but with a different level of irradiation. In Figure 7.22 a results comparison is shown. The temperature trend of both experimental data and numerical prediction between two cases is very similar. An expected constant

gap between the temperatures is present, due to higher radiation that strikes the facade in Case4. Only at 2.0 m in the cavity on the right of the Venetian blind, a difference in the temperature field it is found.

Thus a major analysis has been performed. From the path lines of Figure 7.21 it is evident an irregular flow pattern for Case4, very different from Case3. A direction change of the fluid flow occurs at about $Y = 1.9$ m that brings part of the flow toward the internal cavity and this produces also a variation in the temperature field as shown in Figure 7.22. If the measurement line is moved about 10 cm downward, the trend in the two case is almost perfectly respected.

As a result it is deduced that small variation of the boundary conditions may easily move the zone where flow irregularities occurs. CFD analysis confirms that DSF flow behavior is a challenge for the researcher.

Despite of this consideration, the simulations demonstrate that is possible to apply the decoupling method procedure to the thermal and fluid dynamics analysis of a DSF. Moreover a simplified two–dimensional model produces reliable results, although a three–dimensional model is more accurate and take into account the three–dimensional characteristic of the fluid flow in every zone of the facade.

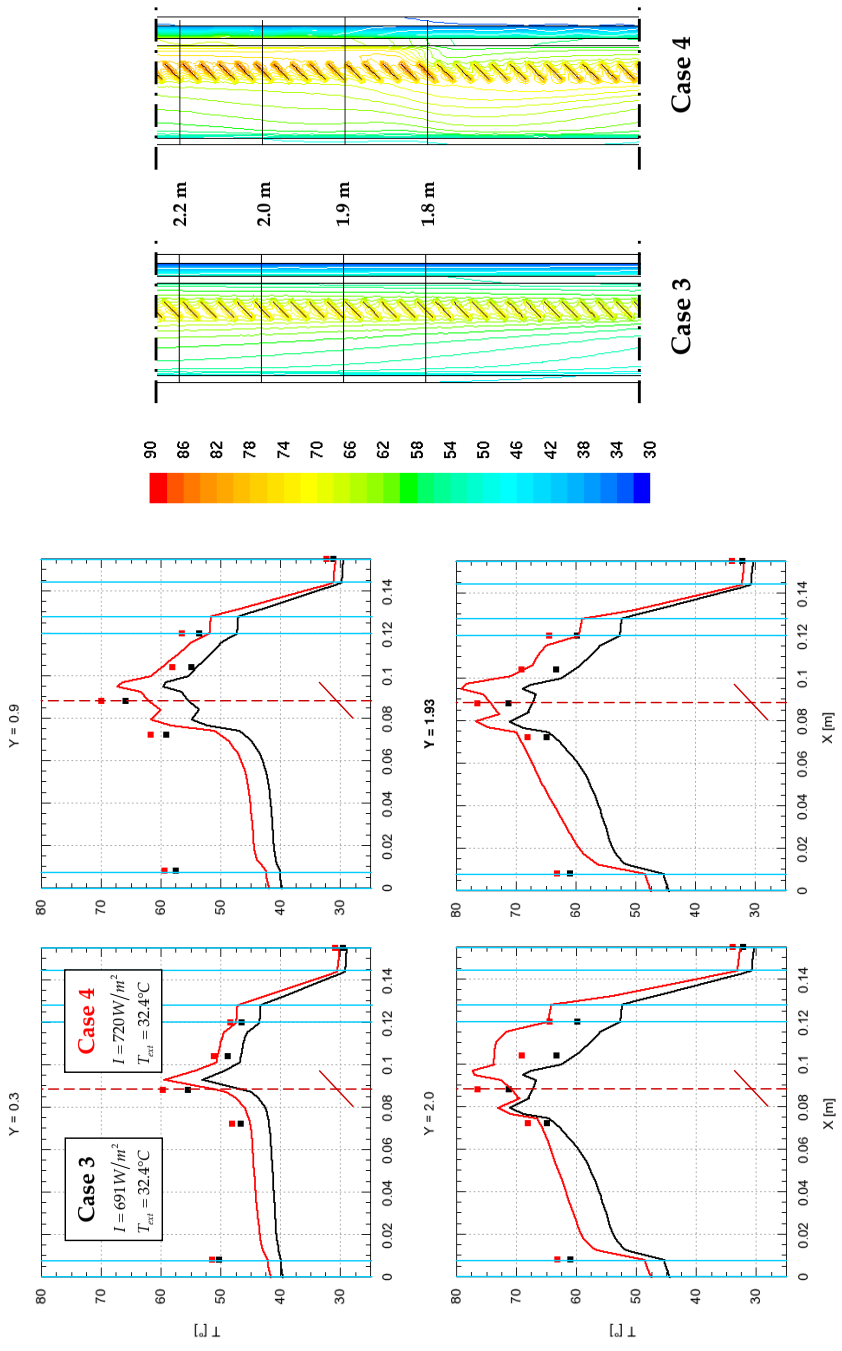

Figure 7.22: *Temperature comparison between Case3 (black) and Case4 (red)*

Chapter 8

Conclusions

8.1 Conclusions

HVAC technology provides several different solutions to reach environmental comfort in buildings, but this is often traduced in a huge cost in terms of energy consumption. Energy saving is now a main objective for researchers. Different thermo-physical phenomena concurs in the building energy balance due to the interaction between the solar radiation and the parts of the building itself.

Fenestration is then one of the main subject concurring to the energy balance. To control solar heat gain and minimize cooling requirements appropriate glazings and shading devices are required. In addiction natural ventilation strategies can reduce energy use for cooling and fresh air requirements.

Architectural trend in the last decade embeds the use of high technology features in the projects for both aesthetic and technical aims. The effort to combine an answer to the international concern about energy and environment problems together with the requirement of aesthetic transparencies in the buildings envelopes, has produced advanced glazing system such as *Double Skin Facades* (DSF).

Unfortunately there are still relatively few buildings in which DSF have been actually realized and till now it has not been possible to completely justify, form a scientific point of view, the real operating behavior. Furthermore the choice of the best typology should be led by the specific location and environmental conditions.

This work produces a comprehensive analysis to understand double–skin facades behavior using a *Computational Fluid Dynamics* (CFD) approach. This method allows a detailed analysis of both flow and thermal fields and provides the representation of the punctual value of every variable in the points of the modeled glazing system.

An experimental approach for the evaluation of DSF performances results in expensive test–campaigns and difficult measurements of important param-

eters. CFD has been chosen as the most reliable tool even if this approach represents a hard challenge due to the very complex thermo-fluid phenomena that characterize the DSF behavior under the different outdoor environmental conditions.

Experimental data, to compare the CFD prediction results, have been provided from Permasteelisa S.p.A R&E Department.

Unfortunately indoor environment systems are usually complicated and experimental data may also contain biased and random error, thus a step–by–step process validation with data from the literature has been performed before proceed with the full analysis. The different aspects of the complex DSF behavior has been individually considered and simulated in the test cases obtaining a good agreement with high quality experimental and numerical data.

Finally a comprehensive analysis of a full DSF system has been provided together with a critical analysis of the results and of the comparisons with the experimental data provided from Permasteelisa.

The DSF has very complex thermo-fluid phenomena under the outdoor environmental conditions, which involve conductive, convective, and radiative heat transfer with laminar, transient, and turbulent flow regimes. To take into account the radiative heat transfer a decoupled method for has been implemented. Firstly, the global net energy balance and the optical properties of the DSF were evaluated from the measured data. Then a CFD software has been used to calculate temperature and flow distributions in the DSF, based on the source terms previously evaluated under different scenarios with varying weather conditions and solar radiation.

The simulation of a complex three–dimensional geometry requires generally high costs in terms of computational time. Thus assumptions and simplifications are commonly adopted when a large number of different simulations are required. Since this work is preparatory to a parametric investigation on DSF, improvement of computational time becomes a relevant criteria for the modeling choices. The first step in this direction has been to perform a grid independence analysis and then to evaluate if the thermal and fluid flows in the facade could be considered two–dimensional.

Despite to the complexity of the flow field, and because the temperature is mainly involved in the purpose of this work, it has been shown that is possible and convenient to assume that the thermal DSF field is two–dimensional.

A comparison between experimental data and numerical predictions has been performed taking into account that only a qualitative analysis is possible due to the lack of informations about measurements accuracy.

As a conclusion, the simulations demonstrate that is possible to apply the decoupling method procedure to the thermal and fluid dynamics analysis of a DSF. Moreover a simplified two–dimensional model produces reliable results, although a three–dimensional model is more accurate and take into account the three–dimensional characteristic of the fluid flow in every zone of the facade.

8.2 Future Works

This research provide a thermal–fluid dynamics analysis of a complete Double Skin Facade and as results it has been possible to affirm that a two–dimensional model is a good compromise between accuracy of the results and computational cost

The work has been developed in order to produce a CFD procedure that could be ready to approach a parametric study of DSF. The mesh size and type, assumptions for the boundary conditions and geometry permits to perform a 2D case simulation in few minutes.

Following step will be the definition of a database for the development of an easy-to-use tool for designers that are approaching DSF without specific thermo–fluid dynamics knowledge. A large number of configuration will be studied, changing individually, in a established range, every parameter that influence the facade behavior.

References

[1] The United Nations Framework Convention on Climate Change. UN - `http://unfccc.int/`, 1997.

[2] ASHRAE. Chapter 31 - fenestration. ASHRAE Handbook-Fundamentals, 2005.

[3] Gratia E. De Herde A. Greenhouse effect in double-skin facade. *Energy and buildings*, 39:199–211, 2007.

[4] Park C. Augenbroe G. Messadi T. Thitisawat M. Sadegh N. Calibration of a lumped simulation model for double-skin facade system. *Energy and Building*, 36:1117–1130, 2004.

[5] Colombari M. Balocco C. Thermal behavior of interactive mechanically ventilated double glazed facade: Non-dimensional analysis. *Energy and Building*, 38:1–7, 2005.

[6] Chen Q. Srebric J. A procedure for verification, validation and reporting of indoor environment CFD analysis. *HVAC&R Research*, 8, no. 2:201–216, 2002.

[7] Chen Q. Srebric J. An example of verification, validation and reporting of indoor environment cfd analysis. *ASHRAE Transaction preprint*, 108, pt. 2, 2002.

[8] Chen Q. Comparison of different k- ϵ models for indoor air flow computations. *Numerical Heat Transfer*, Part B - 28:353–369, 1995.

[9] Blay D. Costa J.J., Oliveira L.A. Test of several versions for the $k-\epsilon$ type turbulence modeling of internal mixed convection flows. *Int. J. of Heat and Mass Tranfer*, 42:4391–4409, 1999.

[10] Niculae C. Blay D., Mergui S. Confined turbulent mixed convection in the presence of a horizontal buoyant wall jet, 1992.

[11] Collins M. Harrison S.J. Naylor D. Oosthuizen P.H. Heat transfer from an isothermal vertical surface with adjacent heated horizontal louvers: validation. *Journal of Heat Transfer*, 124 12:1078–1087, 2002.

REFERENCES

[12] Viskanta R. Zollner A., Winter E.R.F. Experimental studies of combined heat transfer in turbulent mixed convection fluid flow in double skin facades. *Int. J. of Heat and Mass Tranfer*, 45:4401–4408, 2002.

[13] Collins M. Harrison S.J. Naylor D. Oosthuizen P.H. Heat transfer from an isothermal vertical surface with adjacent heated horizontal louvers: numerical analysis. *Journal of Heat Transfer*, 124 12:1072–1077, 2002.

[14] Collins M. Convective heat transfer coefficients from an internal window surface and adjacent sunlit venetian blind. *Energy and Building*, 36:309–318, 2004.

[15] Naylor D. Shahid H. Energy performance assessment of a window with a horizontal venetian blind. *Energy and Building*, 37:836–843, 2004.

[16] Taylor M. Law S. The effect of cavity width on double skin facades. In *International Conference on Building Envelopes System ad Technology*, 2007.

[17] prEN 13119 - Curtain walling - Terminology. CEN, 2004.

[18] Loncour X. Deneyer A. et al. Ventilated double facades - Classification & illustration of facade components, 2004.

[19] Poirazis H. Double skin facades for office buildings. *Lund Institute of Technology - Lund University*, Report EBD-R-0403, 2004.

[20] Belgian Building research Intitute. Source book for a better understanding of conceptual and operational aspects of active facades. department of building physics, indoor climate and building services, belgian building research institute. version no 1. Web address: `http://www.bbri.be/`, 2001.

[21] Uuttu S. Study of current structures in double-skin facades. Master's thesis, Department of Civil and Environmental Engineering, Helsinki University of Technology (HUT), 2002. Web address: `http://www.hut.fi/`.

[22] Saelens D. *Energy Performance Assessments of Single Storey Multiple-Skin Facades - PhD thesis.* PhD thesis, Laboratory for Building Physics, Department of Civil Engineering, Catholic University of Leuven, 2002.

[23] En 12792 - ventilation for buildings - symbols, terminology and graphical symbols. CEN, 2005.

[24] Kragh M. Building envelopes and environmental systems. Web address: `http://www.permasteelisa.com/`, 2000.

[25] Oesterle E. Lieb R-D. Lutz M. Heusler W. *Double Skin Facades - Integrated Planning.* Prestel Verlag: Munich, Germany, 2001.

[26] Lee E. Selkowitz S. Bazjanac V. Inkarojrit V. Kohler C. High-performance commercial building facades. Web address: `http://gaia.lbl.gov/`, 2002.

[27] Gratia E. De Herde A. Natural ventilation in a double-skin facade. *Energy and buildings*, 36:137–146, 2004.

[28] Bohn M.S. Kreith F. *Principle of Heat Transfer – Sixth edition.* Brooks/Cole – USA, 2001.

[29] Compagno A. *Intelligent glass facades - 5th revised and updated edition.* Birkhäuser: Berlin, Germany, 2002.

[30] Trenberth Kihel. EarthŠs annual global mean energy budget. Bull. Am. Met. Soc., 1997.

[31] Yellamrju V. Evaluation and design of double skin facades for office buildings in hot climate - MSc thesis. Master's thesis, Dip. in Architecture, Sushant School of Art and Architecture, Texas A&M University, 2004.

[32] ASHRAE. Ventilation for acceptable indoor air quality. ASHRAE Standard 61, 2001.

[33] Q. Gosselin, J.R. Chen. A dual airflow window for indoor air quality improvement and energy conservation in buildings. *HVAC&R Research*, Accepted, 2008.

[34] Patankar S.V. *Numerical Heat Transfer and Fluid Flow.* Hemisphere Publishing Corporation, 1980.

[35] Fluent inc. *Fluent 6.3 User Guide*, 2007.

[36] Launder B.E. Spalding D.B. *Lectures in Mathematical Models of Turbulence.* Academic Press: London, England, 1972.

[37] Yakhot V. Orzag S.A. Thangam S. Gatsky T.B. Speziale C.G. Development of turbulence models for shear flows by double expansion tecnique. *Phis. Fluid A.*, 4:1510–1520, 1972.

[38] Raithby G. D. Chui E. H. Computation of radiant heat transfer on a non-orthogonal mesh using the finite-volume method. *Numerical Heat Transfer*, 23:269–288, 1993.

[39] Chui E. H. Raithby G. D. A finite-volume method for predicting a radiant heat transfer in enclosures with participating media. *J. Heat Transfer*, 112:415–423, 1990.

[40] Cheesewright R King KJ Ziai S. Experimental data for the validation of computer codes for the prediction of two-dimensional buoyant cavity flows. significant questions in buoyancy affected enclosure or cavity flows. *ASHRAE Winter Meeting*, pages 75–81, 1986.

REFERENCES

[41] Gosselin J.R. A ventilated window for indoor air quality improvement in residential buildings. Master's thesis, School of Mechanical Engineering - Purdue University, USA, 2006.

[42] Oosthuizen P.H. Phillips J., Naylor D. and Harrison S.J. Modeling of the conjugate heat transfer from a window adjacent to a louvered shade. In *Sixth International Conference on Advanced Computational Methods in Heat Transfer*, pages 127–136, 2000.

[43] Colombari M. Interactive wall tests - Test Rooms 5-12 - Preliminary results of full scale monitoring. Technical report, Permasteelisa Research Engineering, 2002.

[44] De Carli M. Colombari M. Involucri edilizi trasparenti a ventilazione forzata: implicazioni impiantistiche. In *58ř Congresso Associazione Termotecnica Italiana*, 2003.

[45] Wis – Advanced Windows Information System. `http://www.windat.org/wis/html/index.html`, 2004 - 2006.

[46] Windat Thematic Network - Windows as renewable energy sources for europe window energy data network. `http://www.windat.org/`, 2001 - 2004.

[47] Klems J.H. Warner J.L. Kelley. A new method for predicting the solar heat gain of complex fenestration system. Final report, Lawrence Berkeley Laboratory – University of California, 1995.

[48] Fedorov A.G. Viskanta R. Turbulent natural convection heat transfer in an asymmetricaly heated, vertical parallel-plate channel. *Journal of Heat and Mass Transfer*, 40:3849–3860, 1997.

List of Publications

Included in Proceedings

Cambuli F., **Fuliotto R**., Mandas N. "Simulazione numerica del flusso su un impalcato da ponte per la valutazione delle derivate aerodinamiche." "CFD simulation on a long span bridge deck for aerodynamic derivatives calculation" 8^{th} Italian National Conference on Wind Engineering – June 2004 – Reggio Calabria - Italy

Fuliotto R., Cambuli F., Mandas N., Bacchin N., Manara G., Chen Q. "Experimental and Numerical Analysis of Heat and Airflow on an Interactive Building Façade" 1^{st} International Conference on Building Energy and Environment (COBEE) – August 2008 – Accepted